ISTANBUL TECHNICAL UNIVERSITY ★ GRADUATE SCHOOL

ABLATION BEHAVIOR AND MECHANICAL CHARACTERIZATION OF 2.5D NEEDLE-PUNCHED HIGH SILICA–PHENOLIC COMPOSITES COMPARED WITH LAMINATED STRUCTURES

M.Sc. THESIS

Zeynep Nur AKYAZICI

Department of Aeronautical and Astronautical Engineering

Aeronautical and Astronautical Engineering Programme

FEBRUARY 2026

ISTANBUL TECHNICAL UNIVERSITY ★ GRADUATE SCHOOL

ABLATION BEHAVIOR AND MECHANICAL CHARACTERIZATION OF 2.5D NEEDLE-PUNCHED HIGH SILICA–PHENOLIC COMPOSITES COMPARED WITH LAMINATED STRUCTURES

M.Sc. THESIS

Zeynep Nur AKYAZICI
(511221215)

Department of Aeronautical and Astronautical Engineering

Aeronautical and Astronautical Engineering Programme

Thesis Advisor: Assoc. Prof. Seher EKEN
Thesis Co-Advisor: Dr. Ceyhun TOLA

FEBRUARY 2026

ISTANBUL TEKNİK ÜNİVERSİTESİ ★ LİSANSÜSTÜ EĞİTİM ENSTİTÜSÜ

LAMİNE YAPILARLA KARŞILAŞTIRMALI OLARAK 2.5B İĞNELEME YÖNTEMİYLE ÜRETİLMİŞ YÜKSEK SİLİKA–FENOLİK KOMPOZİTLERİN ABLASYON DAVRANIŞI VE MEKANİK KARAKTERİZASYONU

YÜKSEK LİSANS TEZİ

Zeynep Nur AKYAZICI
(511221215)

Uçak ve Uzay Mühendisligi Anabilim Dalı

Uçak ve Uzay Mühendisliği Programı

Tez Danışmanı: Doç. Dr. Seher EKEN
Eş Danışman: Dr. Ceyhun TOLA

ŞUBAT 2026

Zeynep Nur AKYAZICI, a M.Sc. student of ITU Graduate School student ID 511221215, successfully defended the thesis entitled "ABLATION BEHAVIOR AND MECHANICAL CHARACTERIZATION OF 2.5D NEEDLE-PUNCHED HIGH SILICA–PHENOLIC COMPOSITES COMPARED WITH LAMINATED STRUCTURES", which she prepared after fulfilling the requirements specified in the associated legislations, before the jury whose signatures are below.

Thesis Advisor :	**Assoc. Prof. Seher EKEN** Istanbul Technical University	.....
Co-advisor :	**Dr. Ceyhun TOLA** Turkish Aeronautical Association University	.....
Jury Members :	**Prof. Dr. Fırat Oğuz EDİS** Istanbul Technical University	.....
	Asst. Prof. Dr. Oğuzcan İNAL Istanbul Technical University	.....
	Assoc. Prof. Dr. Fatih USTA Gebze Technical University	.....

Date of Submission : 26 December 2025
Date of Defense : 02 February 2026

To my family,

FOREWORD

Throughout my master's studies, I would like to express my deepest gratitude to my advisors, Assoc. Prof. Dr. Seher EKEN and Assist. Prof. Dr. Ceyhun TOLA, for their valuable guidance, continuous support, and insightful evaluations. Their constructive feedback at every stage of this thesis strengthened its scientific framework and enhanced the quality of the results presented.

I am also grateful to DeltaV Space Technologies for providing the opportunity to conduct the experimental work within the scope of this thesis and for supporting my efforts in advancing rocket science and the development of materials used in rocket applications. This experience not only strengthened my textile engineering perspective but also enabled me to develop new methods and approaches for aerospace applications. In addition, I would like to thank my manager, Dr. Mustafa BAYSAL, for his valuable guidance and constructive feedback, and Dr. Mehmet KAHRAMAN for his support and contributions throughout the study. I also extend my sincere thanks to our director, Emir ŞEVKİOĞLU, for his support and encouragement during this work. I would also like to express my sincere gratitude to Dr. Mert Hancıoğlu for his assistance and continuous support throughout the composite manufacturing process.Moreover, I would like to extend my special thanks to my colleagues, Burak SELAMET and Muhammed Emin KILINÇ, for their collaboration and assistance during the experiments. I also want to express my gratitude to the specialists at DeltaV Space Technologies, whose invaluable expertise and assistance made the procedure much easier and made a significant contribution at this time.

During this challenging period, I would like to express my deepest and heartfelt thanks to my dear friends, Hande ERTURAN, Şevval SÖNMEZ and Doğa GÜLER, for strengthening my self-confidence, helping me view situations from a broader and different perspective, and making me feel better even during my most stressful moments. Their presence and unwavering support have been among the most valuable sources of strength and comfort throughout this journey.

Finally, I would like to express my love and respect to my mother, Havva AKYAZICI, and my father, Süleyman AKYAZICI, for their endless support and trust in me. I also sincerely thank my brother, Yusuf AKYAZICI, whose guidance and encouragement have helped me advance and grow in engineering throughout this journey. I am deeply grateful to my little pony,Merve AKYAZICI, who has embraced me with love since our childhood and brought joy and strength into my life, and to my little Winnie the Pooh, Sefa AKYAZICI, who is steadily moving toward earning the title of PhD through his academic dedication and achievements. I would also like to thank the person who has always stood by my side in every way and made me feel truly special throughout this period.

February 2026

Zeynep Nur AKYAZICI
(Textile Engineer)

TABLE OF CONTENTS

Page

ABBREVIATIONS

2D : Two Dimensional
2.5D : Two and a Half Dimensional
3D : Three Dimensional
8H : Eight-harness
A-TPS : Ablative Thermal Protection System
C/C : Carbon Carbon
CF : Carbon Fiber
CNT : Carbon Nanotube
C/Ph : Carbon Fiber Reinforced Phenolic
EPDM : Ethylene–propylene–diene monomer rubber
FTIR : Fourier Transform Infrared Spectroscopy
HSF : High Silica Fiber
ILSS : Interlaminar Shear Strength
LAR : Linear Ablation Rate
MAR : Mass Ablation Rate
NA-TPS : Non-ablative Thermal Protection System
NBR : Acrylonitrile–butadiene rubber
NP : Needle-Punched
NNP : Non-Needle-Punched
PBI : Polybenzimidazole
PDMS : Polydimethylsiloxane
PF : Phenol–formaldehyde
RF : Resorcinol–formaldehyde
RVE : Representative Volume Element
RTM : Resin Transfer Molding
SSF : Short Silica Fiber
UD : Unidirectional
UHTC : Ultra High Temperature Ceramics
VARTM : Vacuum-Assisted Resin Transfer Molding
TPS : Thermal Protection System

SYMBOLS

cm	**:** Centimeter
mm	**:** Milimeter
g	**:** gram
g/m^2	**:** Mass per unit area
N/5cm	**:** Peel strength normalized to 5 cm width
MPa	**:** Mega Pascal
kN	**:** Kilo Newton
kg/ m^3	**:** Density
l_i	**:** Initial Thickness
l_f	**:** Final Thickness
m_i	**:** Initial Mass
m_f	**:** Final Mass
t_{burn}	**:** Ablation Time
V_f	**:** Fiber Volume Fraction
°C	**:** Degrees Celsius
%	**:** Percentage
σ	**:** Normal stress
τ	**:** Shear stress
x	**:** Material coordinate
E	**:** Young's modulus
G	**:** Shear modulus

LIST OF TABLES

Page

LIST OF FIGURES

Page

ABLATION BEHAVIOR AND MECHANICAL CHARACTERIZATION OF 2.5D NEEDLE-PUNCHED HIGH SILICA-PHENOLIC COMPOSITES COMPARED WITH LAMINATED STRUCTURES

SUMMARY

The simultaneous physicochemical processes occur both internally and on the surface in materials exposed to high temperature flux and oxidizing/reactive environmental conditions. While temperature dependent decomposition (pyrolysis), phase transformations, and volatile product formation occur within the material, mechanisms such as oxidation, sublimation/thermal decomposition, and flow-induced erosion are activated on the surface. The combined effect of these processes leads to mass and volume loss in both the internal structure and surface of the material. This phenomenon, called ablation, is characterized by material recession and mass loss, especially in thermal protection systems operating under high heat flux. Materials that dissipate heat load by consuming material in a controlled manner through these mechanisms are defined as ablative materials.

In the past, thermal protection materials used in high-temperature environments largely relied on solutions such as monolithic ceramics, refractory metals, and single-phase heat-resistant coatings; however, today, ablative composite materials are widely preferred to simultaneously manage heat load and meet structural requirements. Composite materials offer several advantages thanks to the compatibility of the reinforcement phase (fiber/woven structures) and the matrix phase. These advantages include high specific strength at low density, heat absorption through controlled decomposition (pyrolysis), reduced heat conduction due to the formation of a charred layer on the surface, and the ability to manage damage through specific mechanisms. Therefore, in modern thermal protection systems, ablative composites, especially phenolic-based and textile-reinforced composites, stand out as an approach that provides a higher performance-to-weight ratio and more effective thermal protection compared to traditional monolithic solutions.

However, in laminated composite structures commonly used in ablative composites, volatile products and gas phases formed because of matrix pyrolysis under high temperatures are transported from the material to the surface along the thickness direction (z-direction). The internal pressure created during the escape of gases from the surface, the growth of microvoids, and stress accumulation at the interfaces can lead to weakening of the interlayer bond. In addition, local material loss and mechanical ablation/erosion on the surface caused by gas escape accelerated damage propagation at layer boundaries, increasing the tendency for delamination. Therefore, it is critical to increase not only the in-plane properties but also the out-of-plane (z-direction) strength and toughness under ablation loads. This need is one of the main reasons why architecture capable of providing reinforcement in the z-direction (e.g., two and a half dimensional (2.5D) needle-punched/three-dimensional (3D) textile-reinforced structures) are preferred over laminated structures.

In line with these requirements, reducing delamination and increasing the load-carrying/bonding capacity in the z-direction (thickness direction) of laminated ablative composites has become a critical design objective. High-silica textile reinforcements support insulation performance by limiting heat transfer due to their thermal stability at high temperatures and especially their low thermal conductivity; conversely, phenolic resin consumes endothermic energy through pyrolysis under high heat flux and strengthens the thermal barrier effect thanks to the char layer formed on the surface. However, in classical laminated architecture, internal pressures and interfacial stress generated during the transport of pyrolysis gases in the thickness direction can trigger ply-by-ply separation and delamination due to weak interlayer bonding; this is one of the main damage mechanisms limiting performance, especially in thermal protection system applications where extreme heat loads such as re-entry are encountered in aerospace.

At this point, needle-punch technique stands out as an architectural improvement tool based on textile engineering. Needle punching creates through-thickness fiber bridging by mechanically "locking" high silica fabric layers with silica felt structures along the thickness line; thus, interlayer toughness and load transfer are increased while delamination progression is suppressed. In addition, felt-like porous textile layers can improve the predictability of ablation behavior by providing a more stable surface morphology and more homogeneous damage development during gas release and char formation. Therefore, while maintaining the thermal protection advantages provided by the combination of high silica textile reinforcement and phenolic matrix, mechanical integrity and delamination resistance can be simultaneously improved thanks to the z-directional coupling achieved by needle punching.

This study aims to prevent delamination in high-silica phenolic ablative composites using needle-punch technique and silica felt structure. In high-silica fiber-reinforced phenolic composites, conventional laminated and needle-punched configurations were experimentally investigated in terms of both mechanical response and torch-ablation behavior. High-silica fabric-felt preforms with different fabric/felt layer ratios and approximately the same fiber volume ratios were produced using a laboratory-type needle-punch setup; impregnated with phenolic resin by vacuum-assisted resin transfer molding and consolidated by hot pressing. Tensile, short beam shear, and three-point bending tests were applied for each configuration; in addition, linear and bulk ablation rates were determined using oxy-propane torch tests.

Needle-punched configurations demonstrated a 25–60% reduction in tensile strength and roughly a 25% reduction in flexural strength when compared to the reference laminated structure; however, short beam tests revealed a 40–50% increase in interlaminar shear strength because of better fiber bridging in the thickness direction. While retaining a comparatively high interlayer shear capacity, the silica fabric–silica felt arrangement without needle-punch application only slightly reduced tensile and flexural strength when compared to the reference laminate. This suggests that in situations where process durability and cost are more important than maximum delamination resistance, this more straightforward and easier to manufacture structure might be a viable substitute.

Ablation experiments showed that the layered construction had the highest linear ablation rate and the most noticeable layer-by-layer separation. In comparison to the laminated reference, an optimized needle-punched configuration with a balanced fabric/felt stack arrangement and roughly 60–65% fiber volume ratio decreased the

bulk ablation rate by about 40–50% and the linear ablation rate by about 90% while maintaining comparable levels of tensile and bending performance. According to post-test analysis, needle-punched composites considerably decreased delamination and produced a more stable char layer under intense heat loading.

In conclusion, it was determined that needle-punched high-silica/phenolic composites, with optimized architecture and process parameters, significantly reduced delamination tendency and improved ablation behavior compared to reference laminated structures; however, they maintained acceptable levels in key mechanical performance metrics such as tensile/flexural strength. These findings indicate that these structures are viable and strong candidates for aerospace applications, particularly for thermal protection system components operating under high heat flux.

LAMİNE YAPILARLA KARŞILAŞTIRMALI OLARAK 2.5B İĞNELEME YÖNTEMİYLE ÜRETİLMİŞ YÜKSEK SİLİKA-FENOLİK KOMPOZİTLERİN ABLASYON DAVRANIŞI VE MEKANİK KARAKTERİZASYONU

ÖZET

Yüksek sıcaklık akısı ve oksitleyici/reaktif ortam koşullarına maruz kalan malzemelerde, hem iç bölgede hem de yüzeyde eş zamanlı fizikokimyasal süreçler meydana gelir. Malzeme içerisinde sıcaklığa bağlı ayrışma (piroliz), faz dönüşümleri ve uçucu ürün oluşumu gibi reaksiyonlar gelişirken; yüzeyde oksidasyon, süblimleşme/termal bozunma ve akış kaynaklı erozyon gibi mekanizmalar etkinleşir. Bu süreçlerin birleşik etkisi, malzemenin hem iç yapısında hem de yüzeyinde kütle ve hacim kaybına yol açar. Ablasyon olarak adlandırılan bu olgu, özellikle yüksek ısı akısı altında çalışan termal koruma sistemlerinde malzeme geri çekilmesi ve kütle kaybı ile karakterize edilir. Bu mekanizmalarla kontrollü şekilde malzeme tüketerek ısı yükünü sönümleyen malzemeler ise ablasyon malzemeleri olarak tanımlanır.

Geçmişte, yüksek sıcaklık ortamlarında kullanılan ısı yalıtım malzemeleri büyük ölçüde monolitik seramikler, refrakter metaller ve tek fazlı ısıya dayanıklı kaplamalar gibi çözümlere dayanıyordu; ancak günümüzde, ısı yükünü yönetmek ve yapısal gereksinimleri karşılamak için aşındırıcı kompozit malzemeler yaygın olarak tercih edilmektedir. Kompozit malzemeler, takviye fazının (elyaf/dokuma yapılar) ve matris fazının birlikte çalışabilirliği sayesinde çeşitli avantajlar sunmaktadır. Bu avantajlar arasında düşük yoğunlukta yüksek özgül mukavemet, kontrollü ayrışma (piroliz) yoluyla ısı emilimi, yüzeyde kömürleşmiş bir tabaka oluşumu nedeniyle ısı iletiminin azalması ve belirli mekanizmalar yoluyla hasarın yönetilebilmesi yer almaktadır. Bu nedenle, modern ısı yalıtım sistemlerinde, özellikle fenolik bazlı ve tekstil takviyeli kompozitler olmak üzere aşındırıcı kompozitler, geleneksel monolitik çözümlere kıyasla daha yüksek performans-ağırlık oranı ve daha etkili ısı yalıtımı sağlayan bir yaklaşım olarak öne çıkmaktadır.

Bununla birlikte, ablative kompozitlerde yaygın olarak kullanılan lamine kompozit yapılarda, yüksek sıcaklık altında matrisin pirolizi sonucunda oluşan uçucu ürünler ve gaz fazı, malzeme içinden kalınlık doğrultusunda (z-yönünde) yüzeye taşınır. Gazların yüzeyden çıkışı sırasında meydana gelen iç basınç, mikro boşlukların büyümesi ve ara yüzeylerde gerilme birikimi, tabakalar arası bağın zayıflamasına yol açabilir. Ayrıca, gaz çıkışının neden olduğu yerel malzeme kaybı ile yüzeyde oluşan mekanik aşınma/erozyon, tabaka sınırlarında hasarın ilerlemesini hızlandırarak delaminasyon eğilimini artırır. Bu nedenle, ablasyon yükleri altında yalnızca düzlem içi özelliklerin değil, aynı zamanda düzlem dışı (z-yönü) dayanım ve tokluk kapasitesinin de artırılması kritik öneme sahiptir. Bu gereksinim, lamine yapılara kıyasla z-yönünde takviye sağlayabilen mimarilerin (örn. İki buçuk boyutlu (2.5B) needle-punched / üç boyutlu (3B) tekstil takviyeli yapılar) tercih edilmesinin başlıca nedenlerinden biridir.

Bu gereksinimler doğrultusunda, lamine ablative kompozitlerin z-yönünde delaminasyonunu azaltmak ve yük taşıma/bağlanma kapasitesini artırmak kritik bir

tasarım hedefi haline gelmiştir. Yüksek silika esaslı tekstil takviyeler, yüksek sıcaklıklarda ısıl kararlılıkları ve özellikle düşük ısıl iletkenlikleri sayesinde ısı transferini sınırlayarak yalıtım performansını destekler; buna karşılık fenolik reçine, yüksek ısı akısı altında piroliz yoluyla endotermik enerji tüketir ve yüzeyde oluşan char tabakası sayesinde ısıl bariyer etkisini güçlendirir. Bununla birlikte, klasik lamine mimaride piroliz gazlarının kalınlık doğrultusunda taşınımı sırasında oluşan iç basınçlar ve ara yüzey gerilmeleri, tabakalar arası bağın zayıf olması nedeniyle tabaka tabaka ayrılmayı ve delaminasyonu tetikleyebilir. Bu durum, özellikle uzay ve havacılıkta yeniden giriş gibi aşırı ısı yüklerinin söz konusu olduğu termal koruma sistemi uygulamalarında performansı sınırlayan başlıca hasar mekanizmalarından biridir.

Bu noktada, iğneleme tekniği tekstil mühendisliği temelli bir mimari iyileştirme aracı olarak öne çıkmaktadır. İğneleme işlemi, yüksek silika kumaş katmanlarını silika keçe yapılarıyla kalınlık doğrultusunda mekanik olarak "kilitleyerek" kalınlık yönünde fiber köprüleme oluşturur; böylece tabakalar arası tokluk ve yük aktarımı artarken delaminasyonun ilerlemesi baskılanır. Ayrıca, keçe benzeri gözenekli tekstil katmanları, gaz çıkışı ve char oluşumu sırasında daha kararlı bir yüzey morfolojisi ve daha homojen hasar gelişimi sağlayarak ablasyon davranışının öngörülebilirliğini artırabilir. Dolayısıyla, yüksek silika tekstil takviyesi ile fenolik matris kombinasyonunun sağladığı termal koruma avantajları korunurken, iğneleme ile elde edilen z-yönlü bağlanma sayesinde mekanik bütünlük ve delaminasyon direnci eş zamanlı olarak iyileştirilebilir.

Bu çalışma, iğneleme tekniği ve silika keçe yapısı kullanarak yüksek silika–fenolik ablative kompozitlerde delaminasyonu önlemeyi amaçlamaktadır. Yüksek silika lif takviyeli fenolik kompozitlerde, geleneksel lamine ve needle-punched konfigürasyonlar hem mekanik tepki hem de torch-ablasyon davranışı açısından deneysel olarak incelenmiştir. Farklı kumaş/keçe tabaka oranlarına ve yaklaşık aynı fiber hacim oranlarına sahip yüksek silika kumaş–keçe preformları laboratuvar tipi bir needle-punch düzeneği ile üretilmiş; vakum destekli reçine transfer kalıplama yöntemiyle fenolik reçine emdirilmiş ve sıcak pres ile konsolide edilmiştir. Her bir konfigürasyon için çekme, kısa kiriş kayma ve üç nokta eğme testleri uygulanmış; ayrıca oksi–propan torch testleri kullanılarak lineer ve kütlesel ablasyon hızları belirlenmiştir.

İğneleme uygulanmış konfigürasyonlar, referans lamine yapıya kıyasla çekme dayanımında %25–60 ve eğilme dayanımında yaklaşık %25 oranında azalma göstermiştir; buna karşın kısa kiriş testleri, kalınlık doğrultusundaki daha etkin lif köprüleme nedeniyle tabakalar arası kayma dayanımında %40–50 artış olduğunu ortaya koymuştur. İğneleme uygulanmayan silika kumaş–silika keçe düzenlemesi ise, nispeten yüksek bir tabakalar arası kayma kapasitesini korurken referans laminata göre çekme ve eğilme dayanımında yalnızca sınırlı bir düşüş sergilemiştir. Bu bulgu, maksimum delaminasyon direncinden ziyade proses dayanıklılığı ve maliyetin önceliklendirildiği durumlarda, daha basit ve üretimi daha kolay olan bu yapının uygulanabilir bir alternatif olabileceğini göstermektedir.

Ablasyon deneyleri, lamineyapının en yüksek lineer ablasyon hızına sahip olduğunu ve en belirgin tabaka tabaka ayrılmayı sergilediğini göstermiştir. Lamine referansla karşılaştırıldığında, dengeli bir kumaş/keçe istif düzenine ve yaklaşık %60–65 lif hacim oranına sahip optimize edilmiş iğneleme uygulanmış bir konfigürasyon; çekme ve eğilme performansını benzer seviyelerde korurken kütlesel ablasyon hızını yaklaşık

%40–50, lineer ablasyon hızını ise yaklaşık %90 oranında azaltmıştır. Test sonrası analizlere göre, iğneleme uygulanmış kompozitler şiddetli ısı yüklemesi altında delaminasyonu belirgin ölçüde azaltmış ve daha kararlı bir char tabakası oluşumu sağlamıştır.

Sonuç olarak, mimarisi ve proses parametreleri optimize edilen iğneleme uygulanmış yüksek silika/fenolik kompozitlerin, referans lamine yapılara kıyasla delaminasyon eğilimini belirgin biçimde azalttığı ve ablasyon davranışını iyileştirdiği; buna karşın çekme ve eğilme dayanımı gibi kritik mekanik performans metriklerinde kabul edilebilir seviyeleri koruduğu belirlenmiştir. Elde edilen bulgular, söz konusu yapıların uzay ve havacılık uygulamalarında, özellikle yüksek ısı akısı altında çalışan termal koruma sistemi bileşenleri için uygulanabilir ve güçlü adaylar olduğunu göstermektedir.

1. INTRODUCTION

1.1 Purpose of Thesis

Structural materials are subjected to extremely high heat flux and severe surface abrasion in space and hypersonic flight applications. Under these circumstances, the behavior of the thermal protection layer that isolates and shields the primary load-bearing structure from the environment is just as important to the mission's success as its strength. The Thermal Protection System (TPS), this protective layer, is responsible for controlling surface erosion, managing the heat load that reaches the surface, and preserving the integrity of the underlying structural elements. Because of this, one of the most dependable and straightforward protection methods available today is ablation, which is the controlled dissipation of heat through material recession and mass loss.

However, "which chemical system was used?" is not the only factor that determines an ablative material's performance. The material's internal structure, spatial orientation, bonding between layers, continuity through thickness, and ability to withstand erosion are all equally important. Consequently, multiphase composite systems are typically preferred over single-phase materials in ablative conditions. By fusing the mechanical strength and thermal stability of the reinforcing phase with the binding and load-transferring function of the matrix, composite materials provide superior technical qualities. However, the microstructural organization and dimensional architecture of the components inside the material are the primary factors that define the ablative performance of such materials; the chemical resistance of the components alone cannot account for the performance. Layer alignment, through-thickness fiber connection, porosity distribution, and geometric stability are examples of structural factors that have a direct impact on the composite's mechanical and thermal performance. Therefore, increasing ablative activity can be maximized by engineering the textile architecture, which establishes the dimensional organization of the composite structure, in addition to choosing the right materials.

At this stage, textile-engineered architectures intersect directly with the ablative composite concept widely adopted in aerospace thermal protection systems. Conventional laminated composites are formed by stacking fiber-reinforced plies in prescribed in-plane orientations and exhibit well established mechanical performance at room and intermediate temperatures. Under severe ablative heating, however, the combined effects of matrix pyrolysis, through-thickness gas transport, and thermally induced interlaminar stresses can promote ply-by-ply separation, creating interlaminar voids and progressively degrading load transfer capability and structural continuity. In contrast, 2.5D textile preforms produced via needle-punching and fully 3D textile architectures (e.g., 3D woven structures) introduce reinforcement not only in-plane but also in the thickness direction, thereby enhancing through-thickness connectivity and out-of-plane damage tolerance. By promoting fiber bridging and constraining interlaminar crack growth, these architectures can improve dimensional integrity that allowing the material to remain coherent even as surface recession and mass loss occur. Such through-thickness coupling is therefore critical for preserving both mechanical integrity and geometric stability during ablation, particularly under high heat-flux conditions.

The high silica fiber (HSF) reinforced phenolic composites stands out among the other material systems utilized in ablative composites because of its ability to balance dimensional stability, char formation behavior at high temperatures, and thermal insulation [1]. Silica fibers are an efficient barrier to heat transfer because of their strong melting resistance, low thermal conductivity, and structural stability at high temperatures. In contrast, phenolic resin supports ablative protection by absorbing heat through endothermic reactions during the pyrolytic decomposition process and limiting heat transport through the resultant char layer [2]. When these two constituents are combined in a 3D woven and 2.5D needle-punched textile preform, the material's thickness is continuous, improving the integrity and structural stability of the char layer under severe ablative environments. Therefore, there is a great deal of promise for preserving both mechanical strength and ablative efficiency under high heat flux thanks to this synergy between material chemistry and textile architecture.

The interdisciplinary approach adopted in this study integrates the ablation-based high temperature protection concept used in aerospace applications with textile-engineered through-thickness fiber architectures. The primary objective is to manufacture HSF

/phenolic composites with various needle-punched (NP) configurations and to quantify how these thickness-direction reinforcements affect both mechanical response and ablative behavior. To this end, tensile, three-point bending, and short-beam shear tests were conducted, while oxy–propane torch experiments were performed to determine linear and mass ablation rates. All needle-punched variants were systematically evaluated and benchmarked against a baseline laminated composite under the same test conditions. Overall, this study aims to elucidate the role of textile architecture and component design in the thermal protection efficiency of needle-punched HSF/phenolic composites, and to establish design guidelines that enhance delamination resistance while reducing both linear and mass ablation rates.

1.2 Literature Review

1.2.1 Ablative materials

One of the most important material groups utilized in the aerospace sector to prevent payloads, aerodynamic surfaces, and structural elements from overheating is TPS. The enormous kinetic energy produced at the vehicle's surface during hypersonic flight and atmospheric reentry is transformed into a powerful heat flux when it interacts with the environment. Reradiation and ablation are the two main methods used to eliminate this energy [3]. Based on these two principles, different classes of TPS materials exist as shown in Figure 1.1: non-ablative TPS (NA-TPS) and ablative TPS (A-TPS) materials, respectively [4].

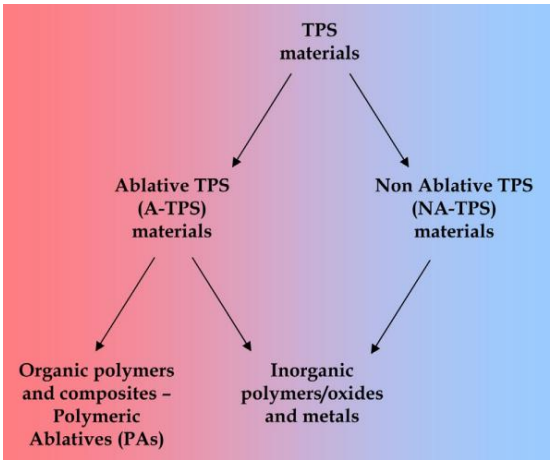

Figure 1.1 : Schematic classification of thermal protection system materials [4].

When heat shields on spacecraft are constructed of non-ablative TPS materials, the primary barrier used to insulate the hull from atmospheric re-entry is reradiation. In this case, NA-TPSs are manufactured using ceramics or certain metals such as tungsten or rhenium. The second mechanism that underpins TPS materials is ablation. The word "ablation" comes from a geological term that means "to move" [5]. While some nonpolymeric materials, like metals, ceramics, and inorganic polymers, have been successfully employed as ablative TPS, polymer-based ablatives represent the most versatile and widely applicable family of ablative materials. This is due to the clear benefits of polymer-based ablative materials, which include low density, excellent thermal shock resistance, superior mechanical strength, and efficient thermal insulation [6].

In this context, carbon, ceramic, elastomeric, and thermoset matrices serve as the foundation for ablative materials. Nonetheless, polymer composites have continued to be the most adaptable heat protection materials since the beginning of space travel. Ultra-high-temperature ceramics (UHTCs) modification has improved the ablation performance of phenolic resins, which have become superior charring binders [7]. Boride and carbide materials based on UHTC, which are notable for having melting temperatures higher than 3000°C, are excellent options for TPS applications. Because of their great strength and formability, these materials are usually reinforced with carbon fibers; nonetheless, CF-reinforced UHTC composites are known to need extra oxidation prevention methods [8].

In elastomeric ablative composites, acrylonitrile–butadiene rubber (NBR) and ethylene–propylene–diene monomer rubber (EPDM) matrices are frequently utilized. These matrices are reinforced with a variety of materials, including carbon fiber (CF), kevlar, polybenzimidazole (PBI), and glass fiber [9-10]. Elastomeric matrices offer a suitable solution for flexible insulation applications requiring high elongation at break [11]. This group's most widely utilized matrix is linear polydimethylsiloxane (PDMS), which breaks down the organic phase under extreme heat to produce a hybrid char structure rich in siliceous and carbon [12]. Polymeric ablatives are the most diversified and adaptable class of ablative materials because of their ability to respond to a wide range of hyperthermal environments. This field of study focuses on altering phenolics, epoxy, phenol–formaldehyde (PF), and resorcinol–formaldehyde (RF) resins to create polymer nanocomposites. RF resins with comparable chemical structures are also

regarded as promising possibilities for next-generation ablative materials, while phenolic resins stand out as superior binders in terms of ablation performance, processability, and cost [6].

In contrast to regular glass fiber and quartz fiber, HSF, a unique kind of glass fiber, demonstrates exceptional thermal resistance and enhanced high-temperature strength. Compared to carbon fiber, HSF offers better thermal insulation performance with reduced conductivity. HSF also provides outstanding ductility and flexibility, making it simple to integrate and process with matrix materials [13].

Consequently, in the thermal environment of hypersonic vehicles, thermal protection composites made of phenolic resin as the matrix and HSFs as reinforcement exhibit outstanding overall performance. Apart from this kind of composite, metal-based, carbon-based, and ceramic-based composites are also frequently utilized in thermal protection systems. In contrast to other composite systems, metal-based composites are mostly used for load-bearing structures that are exposed to relatively modest thermal stresses. However, because of their high density, they need to be processed with extreme precision and surface oxidation prevention. Although carbon-based composites are sophisticated thermal protection materials with high temperature adaptability, they have poor oxidation resistance despite providing good mechanical performance and thermal stability. Oxidation-resistant coatings or matrix impregnation adjustments are frequently needed to improve their environmental adaptability. Ceramic-based composites, available in several configurations, offer excellent high-temperature ablation resistance but are intrinsically brittle, which promotes microcrack growth and limits structural durability. In addition, both carbon- and ceramic-based composites are costly and require complex manufacturing routes, which constrains their widespread engineering use [14].

As a result, ablative thermal protection materials are enhanced constantly, and solutions that better adapt to the task profile, thermal load level, and environmental conditions are becoming increasingly common. In this context, HSF/phenolic composites are featured as a competitive candidate material class due to their cost-effectiveness, suitability for integration with existing production processes, and the balanced performance profile they offer between thermal protection/insulation performance and structural integrity. However, nominal thermal resistance values alone are insufficient for selecting materials that will operate under high temperature

fluxes. First, the dominant ablation mechanisms, such as thermochemical degradation, char formation and erosion, mass loss and surface recession, should be systematically analyzed; the relevant thermal-flow environment and loading scenarios should be defined; and the material architecture and process parameters should be rationally optimized according to the damage/deterioration modes that occur under these conditions.

1.2.2 Ablation mechanism

The majority of the crucial physicochemical features of the ablation process have been identified, despite the fact that it involves very complicated reactions. The heat flux from the hyperthermal environment is initially absorbed by the polymer and subsequently conducted through the material at the start of heating, as schematically shown in Figure 1.2.

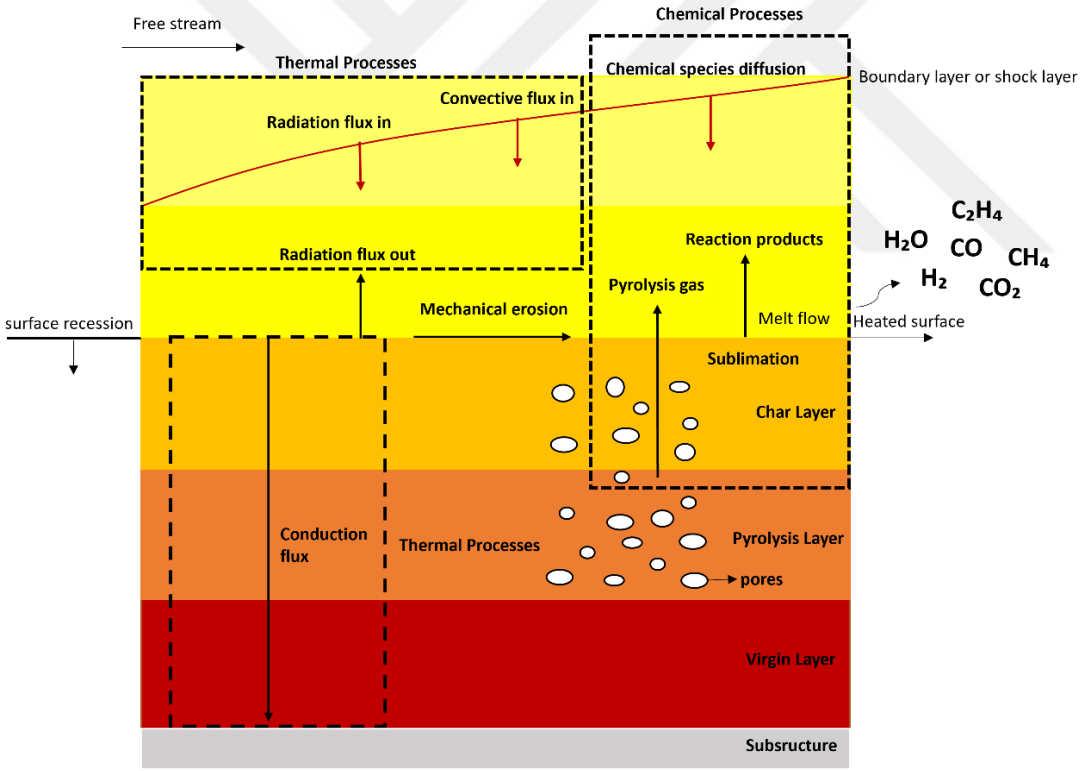

Figure 1.2 : Schematic of heat-transfer modes and material-response mechanisms in an ablative material during high-heat-flux exposure.

The surface temperature determines how quickly heat permeates the material, although thermal diffusion is comparatively slow since polymers have limited thermal conductivity. The temperature rises quickly due to heat retention at the surface region, eventually reaching the vaporization or decomposition temperatures of the substance.

Water, leftover solvents, or low-molecular-weight polymer fragments are often the volatile components emitted in the first stage. At higher temperatures, heat stimulation is enough to break the chemical bonds in the main chain by severing side groups and branching groups connected to the polymer backbone. As a result, the polymer enters a degradation regime in which irreversible pyrolysis processes compete with reversible depolymerization reactions. The degradation rate is determined by the temperature and the amount of still-undegraded (virgin) material and is defined by an Arrhenius-type reaction rate law [15]. In addition to water-gas components like hydrogen (H_2) , carbon monoxide (CO), carbon dioxide (CO_2), and water vapor (H_2O), the gaseous products created during this pyrolysis process can also contain unsaturated hydrocarbons like ethylene and acetylene and saturated hydrocarbons like methane and ethane. These pyrolytic species are transported upwards from the pyrolysis layer through the porous structure, reaching the charcoal region and injecting into the boundary layer (Figure 1.2). In terms of sweating cooling, this gas flow is a critical mechanism for both heat transfer and energy absorption in the near-surface region. The carbon-rich, porous charcoal layer formed above the pyrolysis layer acts as the main thermal barrier protecting the underlying layers against hyperthermal heat flux due to its high effective thermal mass, low thermal conductivity, and high surface emissivity. In addition, endothermic reactions occurring during charring, potential phase transitions, and gas flow create additional heat sinks, increasing total heat absorption. Since a significant portion of the incoming heat load is removed by radiation at high surface temperatures, the net heat flux transferred into the material decreases[16-17].

In most ablation conditions, since the coal seam remains continuously bound to the underlying virgin polymer, pyrolysis and associated pore formation continue beneath the coal seam. This region, where the polymer degrades and porous morphology develops, is defined as the "pyrolysis layer." Pyrolysis gases produced in this region are transported through the porous network to the coal seam; here, they contribute to coal formation while, thanks to the energy they carry, they limit the overheating of the lower layers and support the structural integrity of the deeper virgin structure [16-17].

Figure 1.2 also shows the simultaneous interaction of the coal surface with processes such as oxidation, species transport, radiative/convective heat fluxes, mechanical erosion, and melt flow, if present. In composites containing melt-prone components, the latent heat of melting creates an additional energy sink; high-viscosity melts can

evaporate while remaining on the surface, while low-viscosity melts can flow along the surface. These phase changes and flow regimes are considered as additional mechanisms that increase the total energy consumption during ablation. From a thermophysical point of view, ablation is a multi-physics process in which heat and mass transfer is achieved through controlled loss of surface material, with heat transfer by radiation, conduction and convection; phase changes such as melting, evaporation and sublimation; chemical transformations such as pyrolysis and oxidation; and mass loss processes such as condensation cooling and mechanical erosion working together [16–17].

Although the ablation mechanism is primarily explained by heat-mass transfer and thermochemical degradation, the process simultaneously triggers significant mechanical effects in the composite. Figure 1.3 summarizes the situations that arise at the composite material and composite structure scale under high temperature [18].

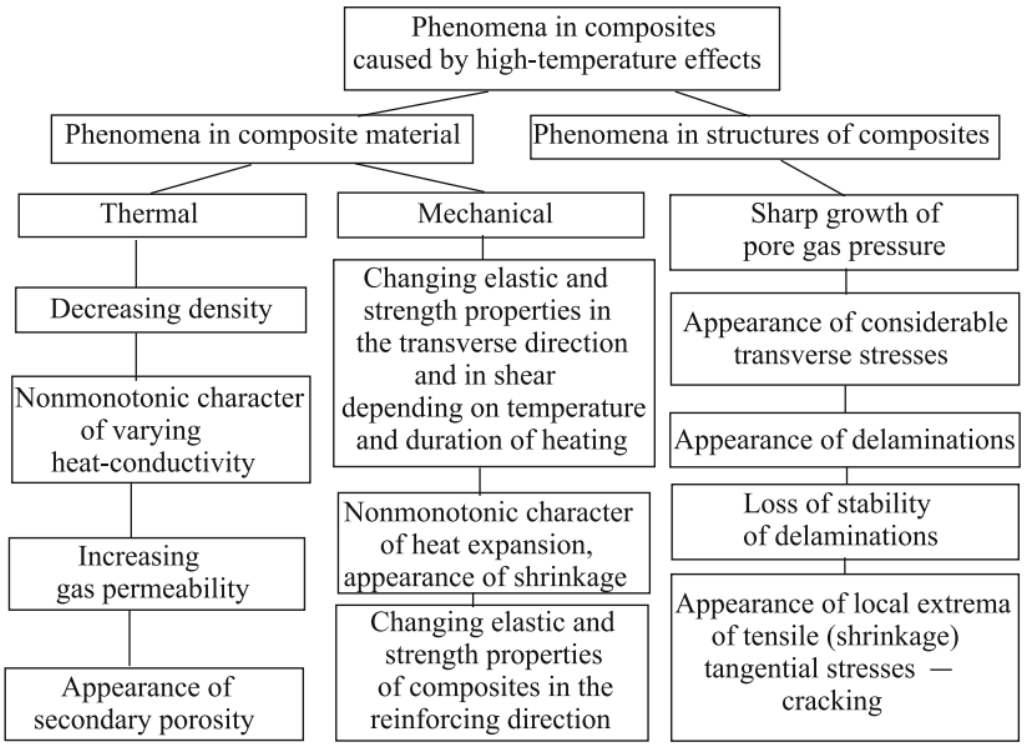

Figure 1.3 : High-temperature-related phenomena in composites [18].

Changes in almost all properties of a material create high temperature effects. Basically, these changes connected to temperature are discussed under two main headings: thermal and mechanical properties. From a thermal perspective, the heating process reduces the density of the composite; thermal conductivity exhibits a non-

monotonic change with temperature; gas permeability increases significantly; and secondary porosity can occur in addition to the primary porosity that develops after technological processes. From a mechanical perspective, exposure to high temperatures and heating duration can significantly alter the elastic and strength properties of composites, particularly in the transverse direction towards the reinforcement and in their shear behavior. However, variations in elasticity and strength parameters along the reinforcement direction are also observed, regardless of the composite type (unidirectional, textile, or laminated structures). Furthermore, thermal expansion behavior can exhibit a non-monotonic character, and additional deformation mechanisms such as shrinkage may occur within specific temperature ranges [18].

When composite materials are used as a structural component and this ablation process is examined, the stress, temperature, and pore gas pressure fields are often non-uniform; the effect of high temperature can redistribute these fields, leading to local pore pressure peaks in the structure, the formation of transverse tensile stresses (σ_{33}) even in thin thermal protective coatings, and the associated risk of delamination. Furthermore, local maxima of tensile/shrinkage stresses in the tangential direction can trigger crack formation. In addition to these effects, surface recession and surface ablation characterized by erosion can develop under the influence of high heat flux and gas jet pressure; this mechanism generally becomes pronounced at temperatures above 1000–1500°C [18].

The key factor determining ablation performance under high temperatures is the continuity and integrity of the char layer formed by the matrix phase during pyrolysis. Therefore, understanding the pyrolysis mechanism of the phenolic matrix is critical in silica-phenolic composites, which are widely used in thermal protection applications due to their high char yield and tendency to form carbonaceous residues after thermal decomposition. However, the structural stability of the composite under high temperatures and the transportability of the char layer are supported by silica fiber reinforcement, which stands out with its high temperature resistance and dimensional stability. Depending on this ablation mechanism, distinct reactions take place when the overall structure of silica-phenolic composites exposed to high temperatures is investigated. The cured structure of the phenolic matrix essentially consists of phenolic units cross-linked through methylene bridges; the objective of pyrolysis is to remove

non-carbon species and obtain a continuous and cohesive carbon char. Literature-based experimental evidence suggests that the phenolic polymer network does not fracture instantaneously upon thermal exposure. Rather, the initial regime is governed by condensation reactions and structural transformations that generate additional covalent linkages and increase crosslink density. As the temperature rises, dehydrogenation and aromatization reactions, together with bond scission events, become dominant, leading to a gradual depletion of carbon-hydrogen (C–H) bonds within the matrix. These findings support the widely adopted representation of phenolic pyrolysis as a three-zone process [19].

1.2.2.1 Region 1 (300-550 °C : early condensation and initial volatiles)

In the initial decomposition stage, the primary volatile products are phenol and cresol from 300 to 550°C. These species are generated by cleavage of terminal benzene rings, with the specific scission position determining whether phenol or cresol is released, as schematically represented in Figure 1.4 [19].

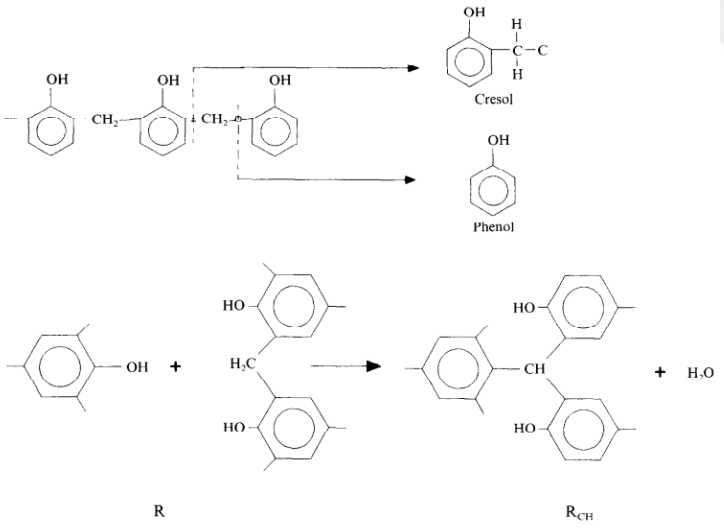

Figure 1.4 : Schematic representation of phenolic resin pyrolysis pathways: bond scission (phenol/cresol formation) and condensation-driven crosslinking with water release [19].

Gas-evolution measurements confirm the onset of phenol and cresol release at temperatures above approximately 300°C. In parallel, water is produced via a condensation reaction between methylene and hydroxyl groups, leaving behind a carbon–hydrogen type crosslink. This water evolution occurs at an early stage of the process, and FTIR (Fourier Transform Infrared Spectroscopy) analysis indicates a

concomitant change in the character of the aliphatic bridging structure . The dominant reactions are in Eq. 1.1 and 1.2 [19] :

$$R \rightarrow R' + Phenol + Cresol \tag{1.1}$$

$$R \rightarrow R_{CH} + H_2O \tag{1.2}$$

where R is the cured resin, R' the resin after pendant ring removal, and R_{CH} the resin containing C–H crosslinks. Region 1 represents the early stage of pyrolysis, characterized by initial crosslink rearrangements, increased interfacial density, and high char reactivity due to remaining oxygenated groups.

1.2.2.2 Region 2 (400-800 °C : ether scission and major gas evolution)

In this temperature region, a second water-forming reaction takes place, where two hydroxyl groups react to generate an ether crosslink from 400°C to 800°C. The amount of water released is somewhat less than half that produced in the first stage. Deconvoluted gas-evolution data clearly show two distinct water-release events, and FTIR confirms that the latter is associated with ether linkage formation from phenolic groups as shown in the Figure 1.5 [19].

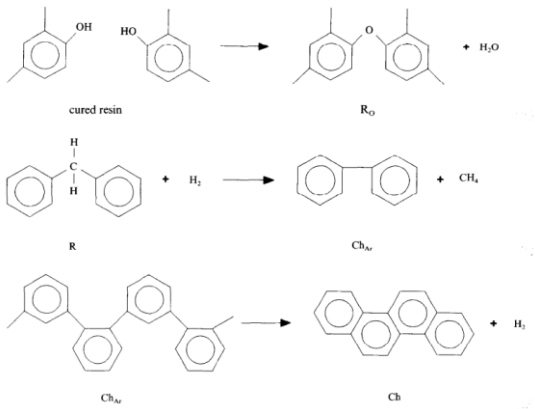

Figure 1.5 : Reaction scheme of phenolic resin pyrolysis and char formation: condensation, aromatization, and carbonization pathways [19].

In this stage, the first hydrogen-evolution peak is attributed to the removal of pre-existing carbon–hydrogen and methylene crosslinks in the cured resin. FTIR spectra show a decrease in aliphatic C–H bonds relative to aromatic C–H, and gas-evolution measurements confirm the release of hydrogen. In the second region, gaseous products

further react with methylene groups: water reacts to form carbon monoxide and hydrogen, while hydrogen reacts with the methylene bridges to produce methane. Additional CO is generated by the breakdown of previously formed ether crosslinks. Both the proposed crosslink-elimination reactions and the evolved species are supported by FTIR and gas-evolution data . Representative reaction pathways are in Eq. 1.3 [19] :

$$\begin{gathered} R \rightarrow R_o + H_2O \\ R_{CH} \rightarrow Ch_c + H_2 \\ R + H_2O \rightarrow CO + H_2 + Ch_{Ar} \\ R_o \rightarrow Ch_{Ar} + O^* \\ R + O^* \rightarrow CO + H_2 + Ch_{Ar} \\ R + H_2 \rightarrow Ch_{Ar} + CH_4 \end{gathered} \tag{1.3}$$

Here, R_O denotes the resin with ether crosslinks, Ch_e the char with C– crosslinks, and Ch_{Ar} the char with direct aromatic–aromatic bonds.

1.2.2.3 Region 3 (560-900 °C : advanced arommatization and char densification)

Due to the cleavage of hydrogen atoms that are directly bonded to the benzene rings, hydrogen is the main gaseous product in the last stage of breakdown from 560°C to 900°C. Accordingly, changes in the ring structure are indicated by peak shifts and variations in relative strength in the FTIR spectra linked to the aromatic ring . The key transformation is in Eq. 1.4 [19]:

$$Ch_{Ar} \rightarrow Ch + H_2 \tag{1.4}$$

where Ch_{Ar} is the aromatic char precursor and Ch is the final stable carbonaceous char. Three successive reaction zones typically describe the high-temperature combustion/pyrolysis behavior of phenolic resin. The ablation response of the composite and the development of the char layer that forms on the surface are mostly determined by these reaction phases. From an engineering standpoint, the applied heating regime can be optimized by quantifying the gas species that generated during pyrolysis and the accompanying reaction rates. Therefore, ablation parameters, especially erosion rate, can be brought within the appropriate range by carefully

regulating the heating rate, allowing for greater process control over the material's service conditions as well as the manufacturing process [19].

Classified as ultra-high temperature fibers, silica fibers are defined as fibers containing 95–100% SiO_2 by weight in their structure. Silica fibers are classified into different subcategories depending on their purity level (in other words, the SiO_2 content in the fiber structure). In this context, they are classified into three main groups: high silica fibers (95–98% SiO_2), pure silica fibers (>99.5% SiO_2), and high-purity silica fibers (99.9–99.999% SiO_2), also referred to as quartz fibers in the literature. Silica fibers are a type of fiber that can maintain their mechanical performance for considerably longer periods at service temperatures reaching up to 1100°C, compared to glass silicate fibers which have higher strength and modulus. Table 1.1 presents the variation in tensile strength of silica and silicate-based fibers at different operating temperatures, as well as the recommended maximum temperature limits for continuous use in practical applications [20].

Table 1.1 : Mechanical strength of high and ultra high temperature fibers [20].

Strength (GPa)	Silicate		Silica		
	E-glass (GPa)	S-glass (GPa)	High (GPa)	Pure (GPa)	Ultrapure (GPa)
RT, (°C)	3,5	4,6	0,4	1,7	2,4
400, (°C)	1,8	3,8	0,2	1,6	1,8
600, (°C)	0,9	2,4	0,1	1,4	1,4
800, (°C)	-	0,7	0,1	1,2	1,0
1000, (°C)	-	-	0,1	0,9	0,9
Cont. Use Rel.Cost.	600 °C	815 °C	1040 °C	1090 °C	1090 °C

The ablative behavior in HSF-phenolic composites is ultimately governed by the thermochemical interactions that take place between the silica fibers and the evaporating phenolic matrix, whereas the three-stage pyrolysis behavior of phenolic resin at high temperature determines the primary reactions of decomposition in the matrix. The silica reinforcement is not entirely inert; the pace at which the fiber/matrix interface is ablated over time is influenced by silanol groups on the surface, softening and viscous flow of the glass phase, and interactions with phenolic char and gas phase products. These interfacial processes determine the development, stability, and permeability of the silica-rich coal skeleton when examining the erosion and thermal insulation behavior of high silica-phenoic composites. When silica (SiO_2) reacts with

carbon during pyrolysis, the following several different ways occur, and as a result, it produces carbon monoxide as a reaction product in Eq. 1.5 [21] :

$$\begin{aligned} SiO_2 + C &\rightarrow SiO + CO \\ SiO_2 + 2C &\rightarrow Si + 2CO \\ SiO_2 + 3C &\rightarrow SiC + 2CO \end{aligned} \tag{1.5}$$

Analysis of test samples did not reveal significant amounts of SiC. This reaction may be omitted. The initial reaction is global in the sense that it is a complex reaction between gases released from solids. It begins with the decomposition of silica, as shown below in Eq. 1.6 [21]:

$$SiO_2 \rightarrow SiO + \frac{1}{2}O_2 \tag{1.6}$$

The carbon and oxygen that are created react. This kind of reaction, which varies depending on the solid's stage of division, may involve diffusion. It is necessary to analyze the behavior of both the matrix and the reinforcement at high temperatures to determine the ablation behavior of a composite. Based on these results, the composite material can be designed according to the desired criteria.

1.2.3 Composite systems for ablative applications

Internal structural components used in aerospace and defense systems require robust thermomechanical protection against extreme thermal environments. This protection is commonly achieved through the use of ablative composite materials, which are specifically engineered to undergo controlled degradation when exposed to high temperatures, thereby dissipating heat and preventing structural failure. Commonly employed in re-entry systems, rocket nozzle assemblies, and thermal insulation components, these materials are designed to withstand thermochemical environments that can exceed 3000 °C and involve extremely high heating rates [22]. Their ability to function under such severe conditions is governed not only by the intrinsic properties of the constituent materials but also by the manufacturing processes employed, which play a decisive role in determining the final thermal and mechanical response.

Using advanced modeling techniques, recent research has focused on assessing the performance of ablative composites by integrating their material composition, manufacturing processes, and high-temperature behavior. In this regard, phenolic resins have gained increased recognition due to their highly crosslinked three-dimensional network structure. In addition to encouraging the formation of a high-carbon char layer that functions as an effective thermal barrier by radiating heat and preventing further degradation at extremely high temperatures, this structure enables them to maintain dimensional stability under thermal stress without softening or melting [23]. The literature has employed a variety of polymer-based material classes for ablative thermal protection. These include low-density coatings (epoxy-novolak systems filled with phenolic microspheres), engine case insulation materials (polybutadiene-acrylonitrile-based mixtures filled with boric acid powder), precarbonized plastics (pyrolized carbon fabric-reinforced phenolic composites), homogeneous plastics (like polytetrafluoroethylene), and filled plastics (like systems with silica powder added to epoxy-polyamide resins). For ablative uses, other comparable polymeric architectures are also being assessed. Variations in component ratios, component types, fiber orientation, processing factors, and manufacturing settings can produce a wide range of attributes within each material class. Table 1.2 provide a summary of room-temperature characteristics for common ablative polymer composites with high and low densities. These statistics show that ablative polymer composites have a broad design range and necessitate application specific tuning of ablation performance, density, mechanical strength, and thermal conductivity [6].

Table 1.2 : Propertie of high-density ablators [6].

Material composition	Phenolic-35%, asbestos mat-65%	Phenolic-35%, silica fabric-65%	Phenolic-50%, nylon fabric-50%	Phenolic-33%, carbon fabric-67%
Density,Ib/ft^3	108	102	72	84
Tensile strength, psi	59,000	9225	6100	21,600
Tensile elastic modulus, million psi	5.06	2.71	1.00	3.50
Tensile elongation at failure, %	-	0.52	2.00	1.08
Shear strength, psi	2210	4410	-	4000
Flexural strength, psi	52,700	23,000	13,100	30,000
Flexural elastic modulus, million psi	5.43	2.9	0.44	2.4

In this context, carbon fiber reinforced phenolic (C/Ph) composites have been widely employed as benchmark ablative materials in the development of thermal protection systems. For instance, the ablative performance of C/Ph composites incorporating carbon black and mesoporous silica fillers has been investigated**.** The reported results indicate that the filler phase significantly influences the thermal protection effectiveness of C/Ph-based ablative composites. In particular, under oxyacetylene torch testing, the specimen containing 20% mesoporous silica exhibited the lowest mass erosion rate, whereas the specimen containing 30% carbon black showed the lowest linear erosion rate and the highest insulation index [24]. Similarly, the ablation resistance of C/Ph systems has been reported to be further enhanced by incorporating zirconium silicide ($ZrSi_2$) particles . The reported findings indicate that the formation of a protective ZrO_2–SiO_2 layer, together with molten SiO_2 on the ablated surface, improves char-layer stability and effectively suppresses oxidation-driven material loss [25]. In parallel, the ablation resistance of phenolic composites has been reported to improve by incorporating a Salen– Nickel (Ni) complex into a boron–phenolic resin. The reported results indicate that in-situ catalytic graphitization occurs during ablation, leading to the formation of a sea–island nanostructured char layer that significantly reduces both linear and mass ablation rates compared with neat phenolic counterparts [26]. Furthermore, the effects of carbon fiber (CF) and carbon nanotube (CNT) reinforcements on the thermal conductivity and ablation behavior of C/Ph composites have been investigated. The reported results indicate that CF- and CNT-modified systems exhibit higher thermal conductivity and improved ablation resistance than random CF/phenolic laminates and neat phenolic resin, as enhanced heat conduction away from the flame front mitigates localized thermal damage during flame-torch testing [27]. Moreover, the ablation resistance and insulation performance of C/Ph composites have been reported to improve by introducing zirconium diboride (ZrB_2) particles. The reported findings indicate that the increased phenolic char yield and the in-situ formation of zirconium dioxide (ZrO_2) and boron trioxide (B_2O_3) phases within the char layer effectively enhance the protective capability under high-temperature ablation conditions [28]. In addition, C/Ph composites have been modified with silicon carbide (SiC) particles, and an SiC content of approximately 5 wt.% has been reported to provide an optimum balance among compressive strength, thermal stability, thermal conductivity, and ablation resistance. Under plasma wind-tunnel testing, the lowest ablation rate was obtained at this filler content response [29].

In parallel with these developments on C/Ph systems, silica fiber reinforced phenolic composites have emerged as attractive candidates for ablative thermal protection, owing to their excellent insulation performance and dimensional stability under severe heating. In a seminal National Aeronautics and Space Administration (NASA) contractor report, systematically analyzed silica cloth/phenolic, graphite cloth/phenolic and graphite cloth/epoxy laminates under simulated rocket oxidizer/fuel environments, combining material-property measurements . The study showed that, for silica cloth/phenolic, the surface recession is controlled primarily by the melting temperature of the silica reinforcement and by the orientation of the woven fibers, rather than by resin content or density alone. Once the surface temperature approaches the silica melting point, a large fraction of the incoming heat is absorbed as latent heat of fusion and by melting of the fibers, which limits the steady-state ablation rate. Owing to the inherently lower thermal conductivity of the silica reinforcement and the resulting thicker, low-conductivity char/melt layer, silica–phenolic laminates exhibited significantly lower back-face temperatures and superior thermal protection compared with graphite–phenolic systems under comparable convective heating conditions [30]. In a more recent study, short silica fiber (SSF)–reinforced phenolic composites have been evaluated under an oxyacetylene flame, and increasing the SSF content from 40 to 55–65 wt.% has been reported to significantly improve anti-ablation performance . In particular, the 55 and 65 wt.% SSF/ modified resole resin (MRR) composites exhibited the lowest linear and mass ablation rates, together with enhanced thermal stability, compared with the neat phenolic matrix, supporting the suitability of lightweight silica–phenolic systems for high-temperature applications [31]. More recently, lightweight hybrid silica–phenolic ablative composites have been developed by combining chopped silica fiber, phenolic resin, and hollow glass microspheres via compression molding . Under argon plasma-jet testing, the addition of glass microspheres has been reported to reduce the mass loss and erosion rates by up to about 48% and 32%, respectively, while increasing the heat of ablation by about 33%. Complementary thermogravimetric and compressive tests further indicated that this three component hybrid system provides improved thermal stability and load-bearing capability for high temperature TPS applications [32].

In conclusion, a review of the literature reveals that ablative composite development has progressed across a wide design spectrum, ranging from basic C/Ph laminates to

particle and catalyst-modified C/Ph formulations and lightweight silica-phenolic architectures. While C/Ph systems continue to serve as reference materials due to their robust carbonization formations and proven performance in challenging environments, silica fiber reinforced phenolics and hybrid variants are becoming attractive for mass-critical TPS applications by providing improved thermal insulation at reduced density. These studies highlight that high efficiency ablative performance is governed not only by component chemistry but also by architecture focused parameters. These include reinforcement morphology and orientation, filler-induced interfacial and char layer reactions, porosity/transport pathways, and microstructural stability under high heat flux. Therefore, achieving an optimal balance between ablation resistance, insulation capability, and mechanical integrity requires an integrated design approach that combines material selection with microstructural and structural architecture approaches.

1.2.4 Influence of reinforcement architecture on ablative performance

For a given matrix chemistry, the reinforcement architecture is one of the most effective design parameters controlling the ablative response of composite thermal protection systems. Recent reviews on polymer based ablative composites highlight that moving from simple unidirectional or two dimensional (2D) woven laminates to more complex 3D orthogonal weaves, braids, 2.5D needle-punched and hybrid textile preforms provides additional degrees of freedom to tailor through-thickness stiffness, delamination resistance and char integrity under severe heating [33-34]. In particular, 3D woven architectures and 2.5D needle-punched architectures have been shown to reduce interlaminar cracking and to improve the stability and permeability of the char layer, thereby influencing both the effective thermal conductivity and the recession kinetics of ablators during high enthalpy flow [35-36]. Consequently, the selection among 2D laminates, 3D woven preforms and 2.5D needle-punched architectures should be regarded not merely as a structural design choice, but as a critical means of simultaneously optimizing the mechanical integrity and ablative performance of next-generation thermal protection systems.

1.2.4.1 Limitations of laminated composites

Classical 2D laminated composites have certain structural restrictions when it comes to ablative thermal protection solutions. 2D fabric layers are stacked to create

conventional layered composites, frequently without reinforcement in the thickness direction. From a fracture-mechanics standpoint, failure in such layered systems arises through several interacting mechanisms, including fiber breakage within a ply, intralaminar cracking in the matrix or along fiber–matrix interfaces, delamination between adjacent plies, and micro or macroscopic loss of stability, with different mechanisms dominating at different stages of the damage process [38-39]. As shown in the Figure 1.6, in addition to delamination, which is commonly seen in laminated composites, various potential forms of damage such as impact, fatigue, fracture, puncture, and corrosion are demonstrated in polymer composites.

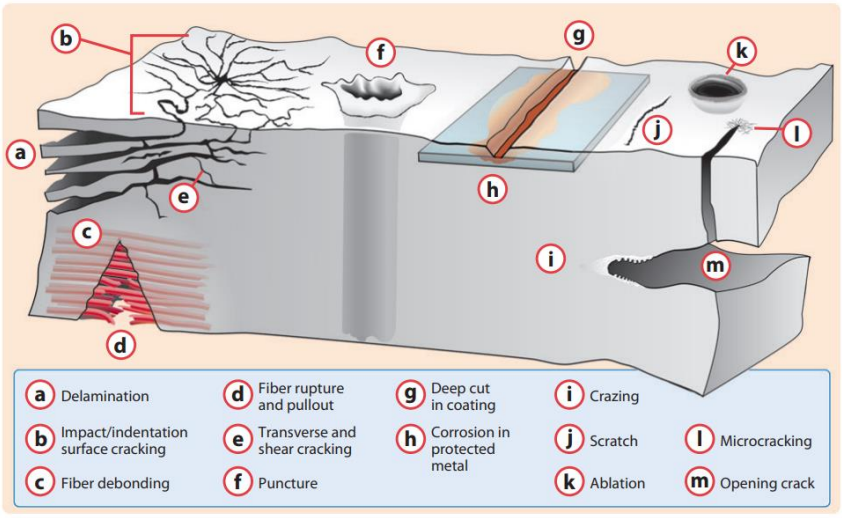

Figure 1.6 : Representative damage modes observed in composites [37].

A closer look reveals that delamination in layered composites is often caused by production flaws from a technological perspective. High residual stresses can result from improper component selection, poor interfacial bonding, variations from ideal curing temperature and time, humidity, press pressure, or wrapping tension. These factors, when combined with operating loads, can cause delamination, particularly in thick-walled parts. As schematically shown in Figure 1.7, high velocity impacts (particle, debris, meteorite) and lower velocity impacts (hail, falling tools, bird strikes, pressure shocks) result in localized damage types like cratering, puncture, penetration, low velocity impact, and pure pressure/temperature loading; all of these conditions are frequently accompanied by delaminations that are invisible from the surface surrounding the impact zone [40].

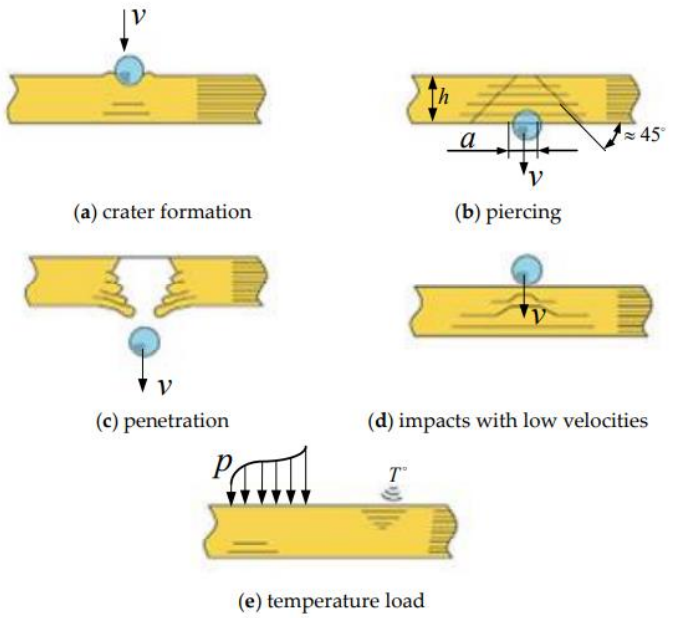

Figure 1.7 : Schematic illustration of impact and thermo-mechanical damage scenarios [40].

Due to the microbuckling effect and the periodic change of stress in the tension-compression direction, these delaminations can grow gradually under cyclic loading. Environmental factors like extreme temperature changes, radiation, moisture absorption, and pre-existing matrix or fiber cracks also hasten the initiation and propagation of delaminations. The critical role of thermally generated interlaminar stresses in initiating delamination has been demonstrated in a number of fracture-mechanics studies on laminated composites. It has been shown that strong through-thickness temperature gradients and free-edge effects can produce singular interlaminar normal and shear stresses that drive delamination growth from small initial defects in angle-ply laminates, even in the absence of severe mechanical loading [41-42]. Analyses on graded multilayer systems further indicate that mismatches in thermal expansion between adjacent layers control the onset of thermally induced interface debonding under heating and cooling cycles [43]. Review studies summarize these findings and emphasize that thermomechanical loading and residual thermal stresses are among the primary drivers of delamination in service. [44]. In the context of ablative thermal protection, experimental and numerical investigations on carbon–phenolic and carbon fiber reinforced polymer (CFRP) ablators have reported ply separation and near surface delamination after arc-jet or rapid heating conditions, confirming that similar thermally driven mechanisms operate under realistic TPS environments [45].

In the coordinate system shown in the Figure 1.8, the x_1 direction is the warp, the x_2 direction is the weft, and the x_3 direction is the thickness direction of the textile composite. According to this definition, the normal stresses σ_{11}, σ_{22}, and σ_{33} in the composite represent the tensile/compressive effects in the x_1, x_2, and x_3 directions, respectively; the shear stresses τ_{12}, τ_{13}, and τ_{23} represent the shear forces in the two respective planes (for example, τ_{13} is the shear in the x_1–x_3 plane) [46].

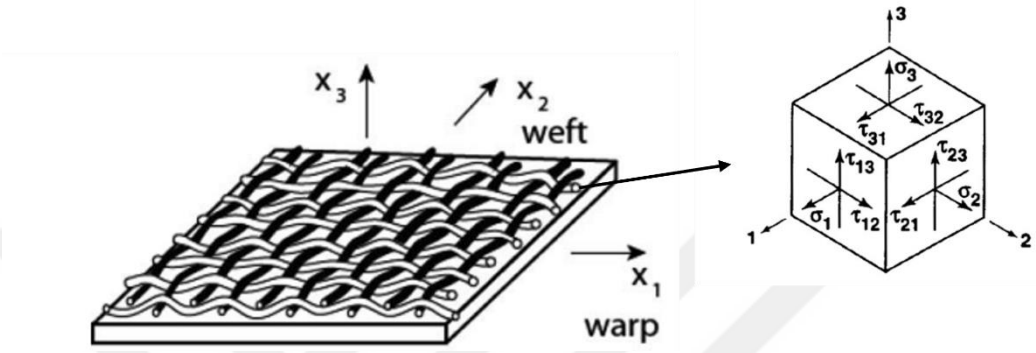

Figure 1.8 : Material coordinate system for a woven composite ply and associated stress components [46].

Upon closer inspection, these textile composite materials at high temperatures can experience different types of failure depending on the type of loading. Accordingly there are six different types of degradation in textile composites at normal and high temperatures: breakage of fabric yarns laid in one of the reinforcing directions, loss of stability of yarns laid in one of the directions, delamination of the composite, and cracking under transverse compression in the direction [18]. Figure 1.9 shows the damage progression of a textile composite under longitudinal tension ($\sigma_{33} > 0$). Initially, the structure is robust; however, as the load increases, shear cracks begin to form in the matrix between the fibers (Figure 1.9b). The primary trigger for these cracks is the multiaxial stress state arising from the curvature of the yarns. In addition to σ_{33}, transverse normal stresses (σ_{11}) and shear stresses (σ_{13}, σ_{12}) increase. When the cracks propagate and coalesce, the process leads to final fracture with the rupture of the monofibers (Figure 1.9c) [18].

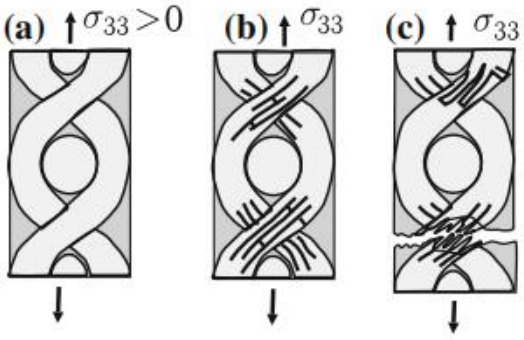

Figure 1.9 : Schematic representation of failure in a textile composite subjected to longitudinal tensile loading: (a) initial intact state, (b) initiation of shear cracking in the matrix between fibres, and (c) ultimate fracture due to monofibre rupture [18].

Figure 1.10 summarizes how damage develops under longitudinal compression ($\sigma_{33} < 0$). In compressive loading, damage does not begin with direct fiber rupture as in tension; rather, it begins with local stress concentrations in the regions where the yarns are most twisted and shear damage/local instability in the matrix. Therefore, compressive strength is determined by the effect of σ_{33}, along with the curvature-induced σ_{11} and shear components; maximum effects occur. This approach provides a fracture criterion consistent with the "matrix-shear crack initiation" mechanism in Figure 1.10b for tension and the "local shear damage/instability" mechanism for compression [18].

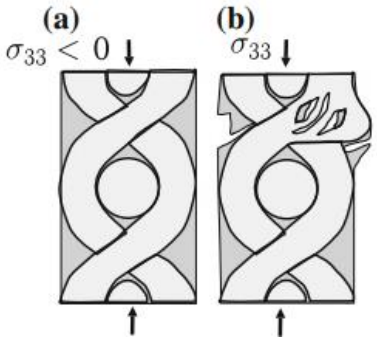

Figure 1.10 : Schematic damage model textile composite under longitudinal compression [18].

Figure 1.11 summarizes the development of damage in the composite under transverse tension ($\sigma_{11} > 0$). Initially, the structure is undamaged (Figure 1.11a); however, as σ_{11} increases, stress concentration occurs at the fiber/matrix interfaces and between layers. In this case, interlayer cracks begin in the matrix, particularly under the

influence of the shear component σ_{13} (or τ_{13}) which is bonded along the thickness, and delamination occurs as the cracks progress (Figure 1.11b) [18].

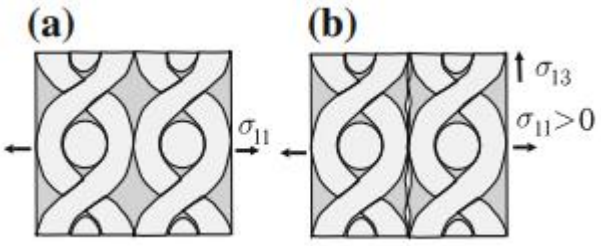

Figure 1.11 : Schematic representation of failure textile composite subjected to transverse tensile loading: (a) undamaged composite, (b) initiation of interlayer cracking in the matrix and subsequent delamination [18].

Figure 1.12 shows the damage mechanism observed under transverse compression ($\sigma_{11} < 0$). In the undamaged condition (Figure 1.12a), the layers maintain their arrangement; however, under compressive load, the matrix begins to crack in the interlayer region due to shear stresses. As loading continues, these matrix shear cracks propagate between the layers, and the structure undergoes progressive destruction with local crushing/deterioration (Figure 1.12b) [18].

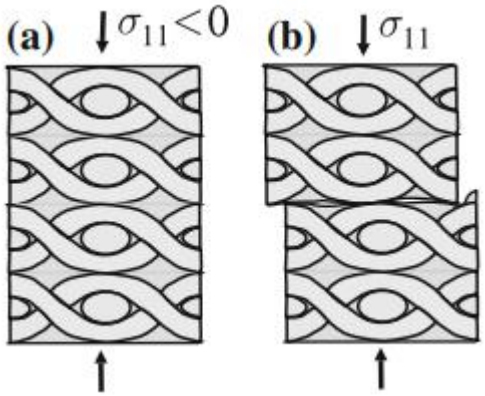

Figure 1.12 : Schematic illustration of failure textile composite subjected to transverse compressive loading: (a) intact state, (b) development of matrix shear cracks between fabric layers followed by progressive destruction [18].

Woven fabric ply, because it mostly has a 0°–90° fiber arrangement, behaves more stably in the x_1 and x_2 directions; that is, it can exhibit similar stiffness and strength in these two directions. In contrast, since the fibers remain largely within the plane, the stiffness and strength in the thickness direction (σ_{33}, τ_{13}, τ_{23} related to x_3) are generally lower. In practice, this is one of the main causes of damage such as delamination: under stresses such as external plane loads or gas pressure/shear effects,

the stresses related to x_3 increase in the interlayer region, and a tendency to separate arises due to the poor thickness strength.

Therefore, the low out-of-plane (x_3) stiffness and strength of the woven fabric layer makes delamination a critical damage mechanism in cases where the σ_{33}, τ_{13}, and τ_{23} components are increased in the interlayer region. Indeed, the literature shows that conventional 2D laminated abrasive materials are structurally vulnerable to thermally induced layer separation under high temperature gradients and internal pressures created by pyrolysis gases throughout the thickness. To mitigate this weakness and improve the structural and abrasive integrity of thermal protection systems, advanced textile architectures such as 3D weaving and 2.5D needle-punch, which provide reinforcement along the thickness, offer a strong rationale for a solution.

1.2.4.2 Development of textile-based architecture

As schematically illustrated in Figure 1.13, textile reinforcements used in composites have a hierarchical structure. At the lowest level, individual fibers (staple or filament) are gathered into slivers or rovings and then converted into yarns by spinning and twisting, with yarn fineness commonly expressed in tex, denier or related units.

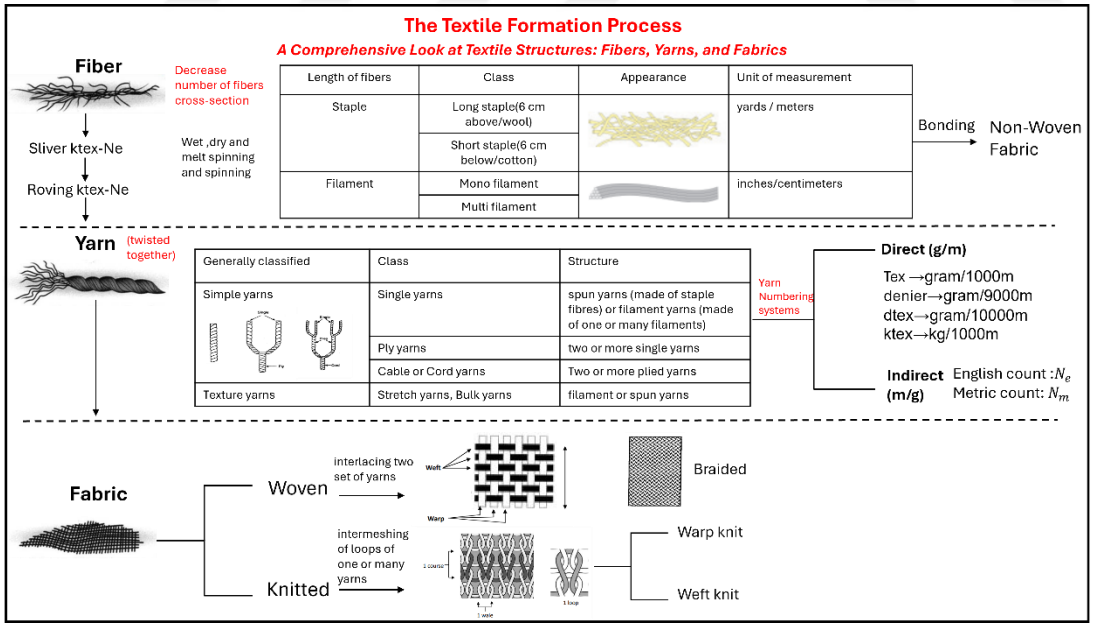

Figure 1.13 : The textile formation process.

At the fabric level, these yarns are organized into different textile architectures, such as woven fabrics (interlacing warp and weft yarns), knitted fabrics (intermeshing yarn loops), braided structures (intertwining yarns along inclined paths), and non-woven

felts obtained by bonding fiber webs. Each of these architectures can be realized in essentially 2D form, where fiber paths lie predominantly in the plane of the fabric, or in 3D configurations, where additional through-thickness yarns or needled fibers provide fiber continuity in the thickness direction. This hierarchical view of textile formation is essential for understanding how reinforcement architecture can be tailored to improve the through-thickness behavior and ablative performance of composite materials.

Among the various textile architectures, woven fabrics are of particular interest in this study, since they provide a well-defined arrangement of warp and weft yarns, can be manufactured in both 2D and 3D forms, and are widely used as primary reinforcements in high-temperature composite ablators. As illustrated in Figure 1.14, woven fabrics are produced by interlacing two orthogonal yarn systems, warp (0°) and weft or filling (90°), following a periodic weaving pattern. Fabric integrity is maintained by the mechanical locking of these yarns at the crossover points, while global properties such as drape, in-plane stiffness, porosity, and surface smoothness are governed by the selected weave style and processing parameters [47-48].

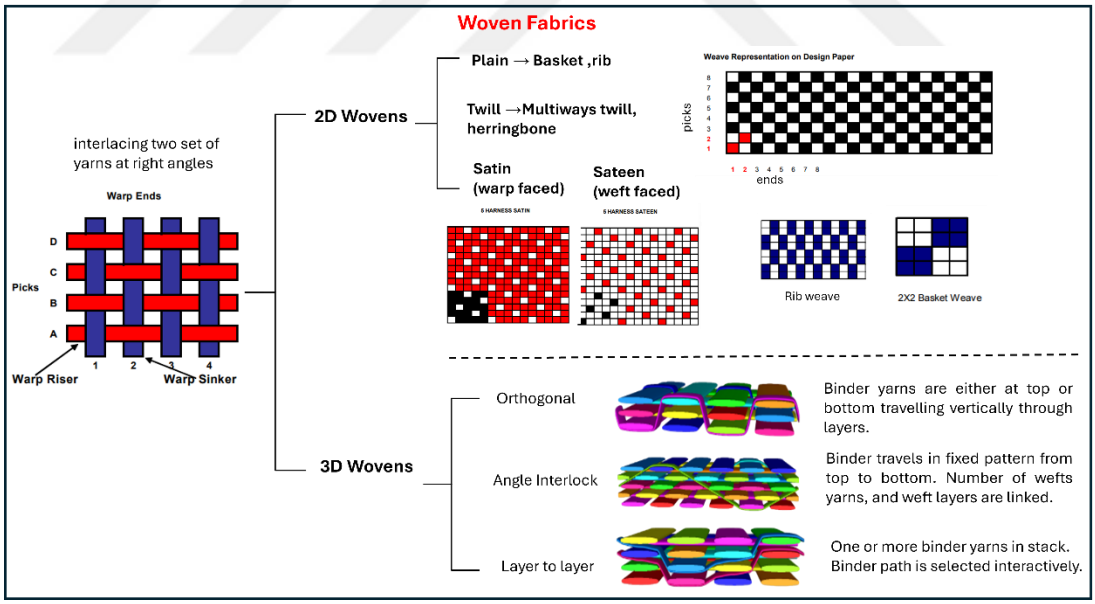

Figure 1.14 : Schematic representations of woven-fabric architectures.

The simplest structure is the plain weave, where each weft yarn alternately passes over and under successive warp yarns and each warp behaves analogously. This produces a structurally balanced and relatively porous fabric with high dimensional stability but pronounced yarn crimp, which can reduce the effective in-plane stiffness of the

resulting composite. A balanced fabric has the same yarn count and the same number per unit length in the warp and weft yarn system. So that plain-weave fabric has a seemingly similar face and back because of the uniform warp and filling interlacing. At the same time, rib fabrics are named unbalanced plain weaves. They are distinguished by the presence of crosswise ribs or ridges on the fabric's face and back. Basket weave is a plain weave that interlacing more than one warp yarn with more than one filling yarn. In addition, when a few textiles consist of two or three warp yarns floating over one filling yarn, they are half-basket weaves [47-48].

In twill weaves, the interlacement points are shifted from one yarn to the next, generating a characteristic diagonal pattern that improves drape and conformability at the expense of a slight reduction in in-plane stability. The diagonal lines on the fabric's surface can be seen to run either upward to the right, which is referred to as a "Z twill" or "right-hand twill," or in the opposite direction, which is referred to as an "S twill" or "left-hand twill," when viewed along the warp direction as shown in the Figure 1.15. Due to their pattern structure, twill fabrics have longer yarn transitions and fewer crimp points compared to plain fabrics with similar properties [47-48].

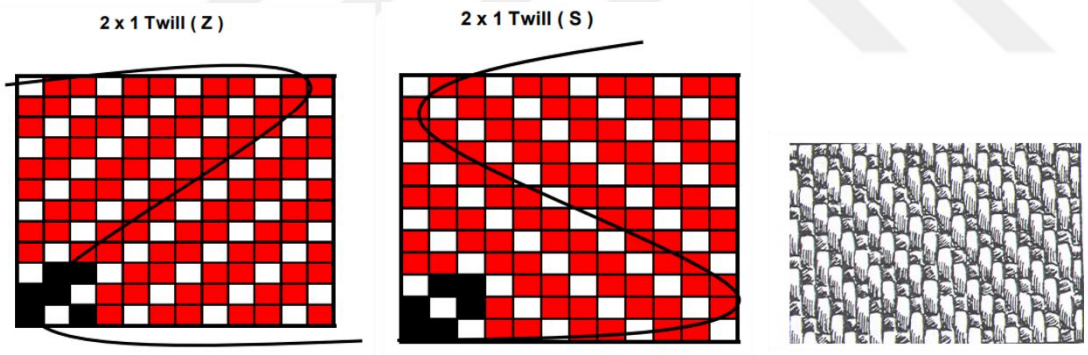

Figure 1.15 : Weave diagrams of 2×1 twill fabrics with Z- and S-direction twill lines, with a representative fabric surface appearance [47-48].

Satin and sateen weaves, in which yarns float over several cross yarns before interlacing, yield smoother surfaces, higher cover factors, and tighter fabrics and are often selected when good impregnation and improved mechanical performance are desired. Satin fabrics are generally uneven and contain fewer interweaves per unit area and have fewer crimp points compared to plain weave and twill fabrics. Spun yarns are the main component of sateen, a derivative structure of satin cloth. The strands that float on the fabric face are the filling yarns in this structure, which is usually a filling-faced satin weave as shown in the Figure 1.16 [49] .

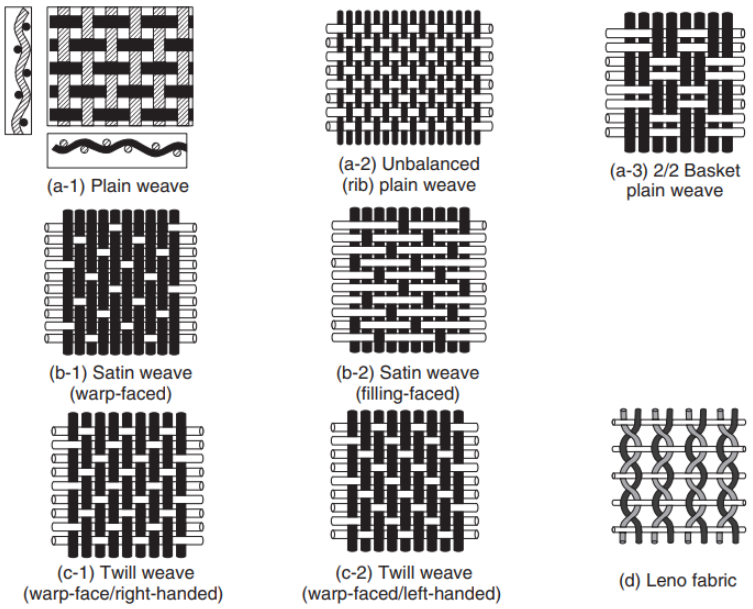

Figure 1.16 : Schematic representations of common woven-fabric weave patterns [49].

In satin fabrics, each warp and weft yarn is tied only once within the repeat; therefore, satin/sateen fabric requires a repeat of at least five yarns, and the fabric is named according to the repeat size used, such as 5-harness, 8-harness, etc. In this structure, the term harness refers to the number of shafts (heddle shaft/harness frame) in the weave's repeat, and thus the binding pattern; for example, the expression 8-harness satin (8H) indicates that the pattern repeat is constructed from 8 warp yarns (and correspondingly 8 heddle shafts) [50]. As the number of harnesses increases, the attachment points are distributed more sparserly within the report, increasing the float length and giving the surface a smoother character. The 8H satin pattern is created by regularly shifting the bonding points throughout the report according to the ‘satin progression/step’ (base) rule; this approach prevents bonding points from overlapping, ensuring a homogeneous float distribution on the surface. Satin weave layers are inherently asymmetrical; warp yarns dominate on one surface, while fill/weft yarns dominate on the other. Due to this asymmetry and the non-symmetrical nature of yarn exchange regions as shown in the Figure 1.17, twisting and elongation behaviors can become correlated within a single satin layer; furthermore, an interaction can occur between elongation and in-plane shear [51].

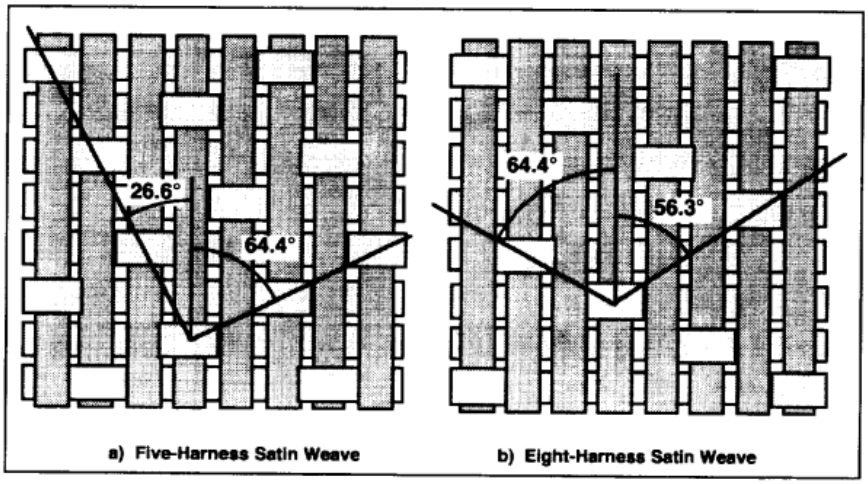

Figure 1.17 : Diagonal patterns generated by the exchange regions and their corresponding angles [51].

In multilayer laminates, this effect can be reduced by considering which side of each layer faces the mold; furthermore, satin weaves offer high drape/conformability thanks to their long flocs. This trend has also been reported in the literature. It has been shown that in-plane shear strength increases as float (uncrimped yarn length) increases for different weave types. As seen in Figure 1.18, oxford weave has the shortest float length, followed by 5-harness satin and 8-harness satin; it is observed that the in-plane shear strength value increases with the increase in float length. Therefore, the preference for 8H satin structure in this study is related to the assumption that its low crimp and long float characteristics can provide advantages in terms of in-layer shear behavior and impregnation performance during production [51].

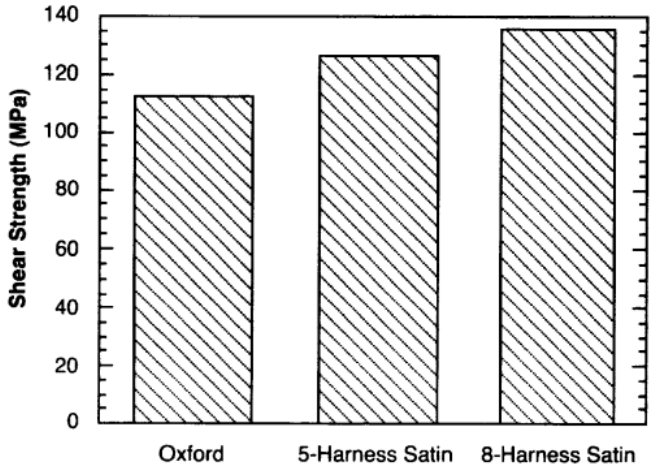

Figure 1.18 : In-plane shear strength comparison among different weave architectures, highlighting the influence of crimp [51].

As summarized in Figure 1.19, the performance of woven reinforcements is not only governed by the weave pattern itself but also by a set of fundamental geometric parameters at the fabric scale.

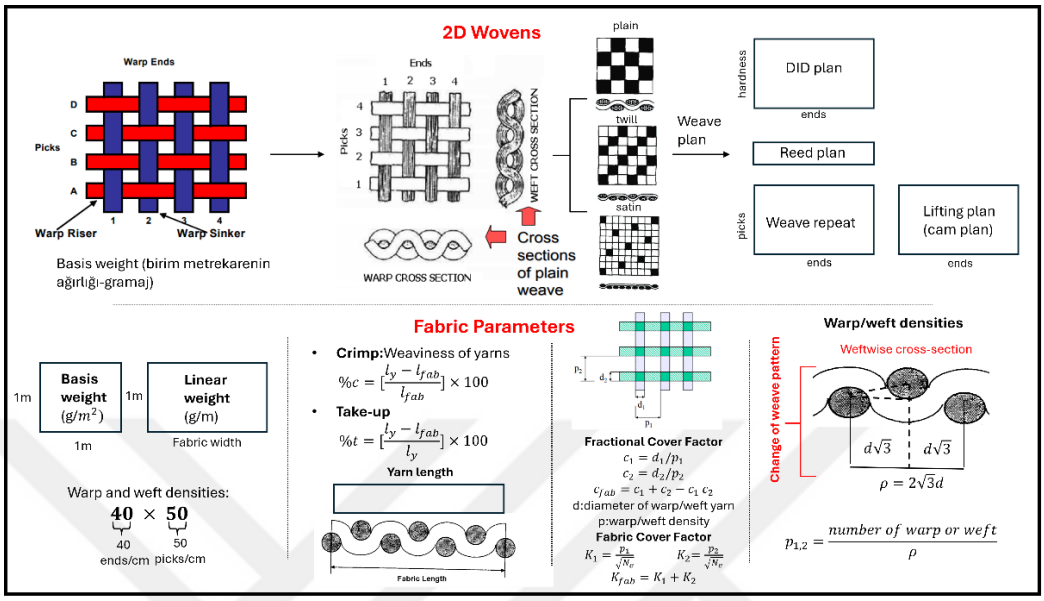

Figure 1.19 : 2D woven fabric architecture and representative structural parameters used for geometric characterization.

The areal density (basis weight), yarn linear density, and warp/weft counts (ends and picks per unit length) jointly determine the fiber volume fraction and thickness of the fabric. Yarn crimp, defined as the relative waviness of warp and weft, controls the balance between stiffness and conformability: increasing crimp generally reduces the tensile stiffness and strength of the resulting composite but improves drape and in-plane permeability by opening inter-yarn channels. The warp and weft cover factors, obtained from yarn counts and yarn diameter, quantify how much of the fabric surface is actually occupied by yarns and therefore govern porosity, air/resin flow, and thermal transport through the preform. Recent experimental and modelling studies have shown that systematic variation of these parameters particularly crimp level, weave density, and cover factor strongly affects mechanical response, permeability, and damage evolution in woven composites and must therefore be considered together with 2D, 2.5D, and 3D reinforcement architectures when designing textile-based ablative materials [48].

3D woven architectures in the Figure 1.22 extend this concept by adding binder yarns that traverse the thickness direction. In orthogonal 3D weaves, warp and weft layers are tied by near-vertical binders normal to the fabric plane, whereas angle-interlock

designs route binders along inclined zig-zag paths to interlock multiple weft layers, and layer-to-layer weaves connect adjacent layers selectively. Compared with 2D weaves, these 3D configurations minimize discrete ply interfaces and markedly improve through-thickness strength, damage tolerance, and delamination resistance key advantages for textile-reinforced ablative composites [52]. In recent years, 2.5D and 3D woven architectures have become a central focus for advanced thermal protection systems, with several woven TPS concepts exploiting orthogonal and angle-interlock designs to tailor through-thickness strength, thermal conductivity, and local fiber volume fraction for specific entry environments [53]. The Extreme Entry Environment Technology (HEEET) concept employs a dual-layer 3D woven carbon/phenolic architecture that combines a dense, oxidation-resistant outer layer with a low-density insulating inner layer, and has demonstrated robust performance and mass efficiency in arc-jet and design studies for extreme planetary-entry probes [54]. Beyond these mission-specific systems, multiscale modelling and optimisation studies on 3D woven TPS materials indicate that exploiting orthotropic thermophysical properties and graded weave designs can improve heat-shield insulation while reducing areal density by more than about 10–15 % relative to isotropic or quasi-2D solutions [55-56]. These developments demonstrate that 3D woven reinforcements represent the current advanced textile architecture for abrasive TPS and provide an integrated way to simultaneously improve integrity, damage tolerance, and thermal protection efficiency throughout the thickness.

Despite these advantages, conventional 3D woven preforms still face practical limitations in large-scale TPS manufacturing because of their complex weaving routes, low automation efficiency, and relatively high production cost. Nevertheless, their periodic Z-direction yarn paths provide excellent through-thickness strength and interlaminar bonding, which significantly enhance ablation and delamination resistance. Motivated by the desire to retain these benefits while reducing process complexity, so-called 2.5D needle-punched preforms have gained considerable attention in recent years. In these architectures, bundles of fibers are needled in the Z-direction through a stack of successive 2D woven plies in the XY plane, creating a quasi-3D reinforcement. Owing to their lower manufacturing cost, high design flexibility, and straightforward integration with automated production lines, 2.5D

needle-punched textile composites are increasingly being adopted in aerospace and defense applications as an attractive alternative to fully 3D woven ablators [57].

1.2.4.3 Needle-punched composites

Needle-punching is a mechanical through-thickness reinforcement technique in which barbed needles reciprocally penetrate stacked fibre layers, as illustrated in Figure 1.20. During penetration, the barbs capture surface fibres and transport them in the thickness (z) direction; upon withdrawal, part of the fibres remain as loops/bundles, effectively stitching adjacent layers and creating z-directional fibre bridging. The resulting through-thickness connectivity can be tailored by adjusting key parameters such as punch density, penetration depth, and the imposed punch pattern (including periodic regions and preform rotation) [57-58].

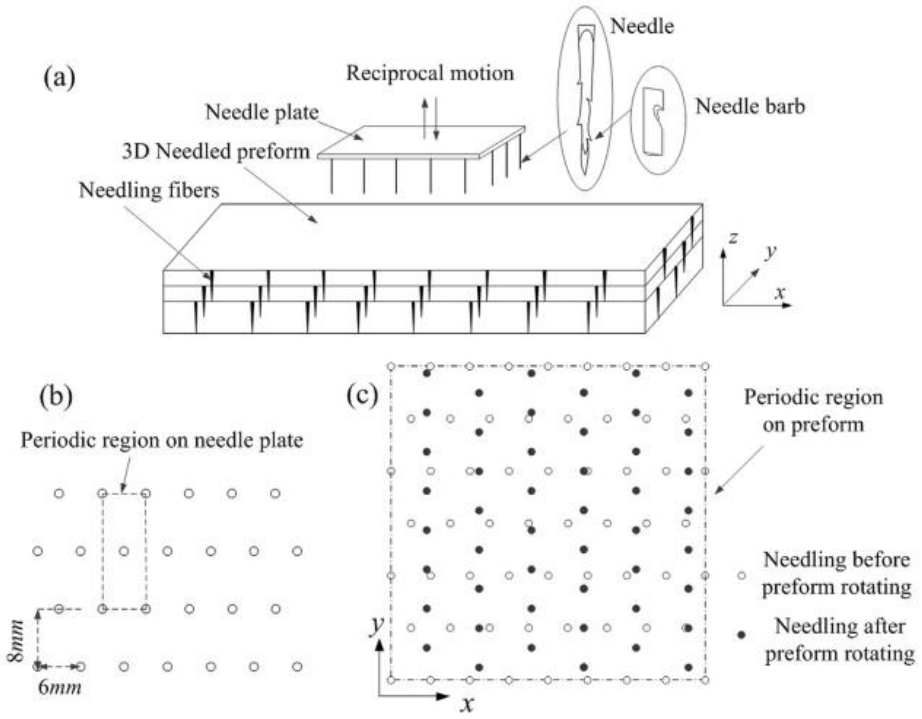

Figure 1.20 : Schematic of the needle-punching process and punch-pattern strategy: (a) barbed needle penetration through the preform, (b) periodic region on the needle plate, and (c) periodic needling pattern on the preform before/after preform rotation [58].

In fact, needle punching is one of the fundamental mechanical bonding methods used in nonwoven textile manufacturing, and nonwoven structures produced by this technique are commonly referred to as felt in the literature. As schematically shown in Figure 1.21, the loose fibre web is continuously conveyed by rollers, while a

reciprocating needle board repeatedly penetrates the batt to entangle fibres through the thickness and consolidate the structure into a coherent nonwoven layer. Needle-punched felts offer a medium that makes it easier for the serrated needles to catch and drag the fibers in the Z direction since they are made of randomly oriented fibers and have a clearly heterogeneous microstructure with a wide pore size range [59-60].

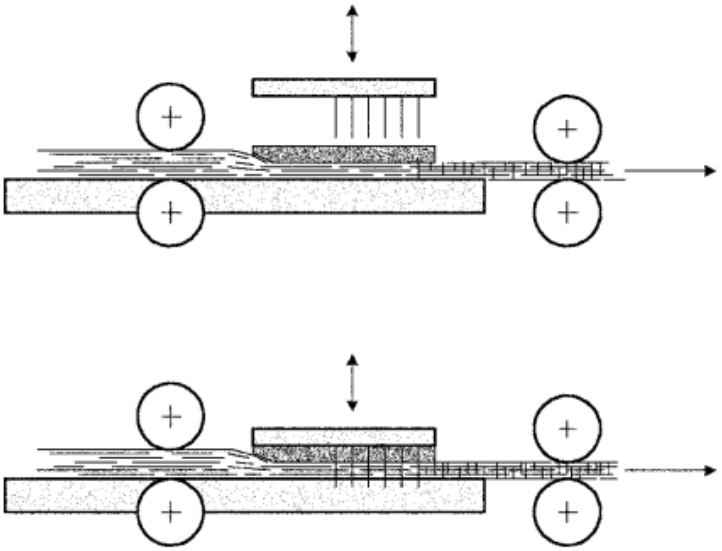

Figure 1.21 : Schematic of an industrial needle-punching line for nonwoven production, illustrating web feeding/transport by rollers and reciprocating needle penetration through the fibre batt [59].

However, in 3D woven structures, the binding yarns continuously interlock all warp and weft layers in the Z direction, whereas in needle-punched structures, the fibers carried by needle-punching only bridge a limited number of layers, creating local connections and not providing complete continuity throughout the entire volume. Therefore, although this architecture has a more three-dimensional character than classic 2D laminates, it is classified as 2.5D because it does not offer the same volumetric connection as fully woven preforms [59-60].

It is possible to produce preforms with different architectures using the needle-punch technique. In this method, hybrid preform configurations can also be created by using felt (nonwoven web) and stacking it with unidirectional or 2D woven fabrics. The primary function of the process is to allow the staple fibers in the felt to penetrate the woven fabric layers by being transported in a Z direction via serrated needles. Thus, a mechanical “stitch” effect is created along the thickness line between the in-plane

(XY) fibers of the fabric and the randomly oriented fibers in the felt, and the interfacial integrity is significantly strengthened by the through-thickness bonding of the preform.

There are studies in the literature regarding both the definition of the geometric parameters of the needle-punch process and the evaluation of ablative performance under high-temperature conditions. For example, the effect of needle-punching parameters on the effective material properties of 3D needle-punched carbon/carbon-silicon carbide (C/C–SiC) composites was numerically investigated. A periodic unit cell representing needle-punched and unneedled regions was established based on microstructure observations; fiber fracture, fiber deflection, and pinhole geometry were included in the model. The analytical/numerical results were found to be consistent with experimental data, and it was shown that needle punching density, depth, and distribution significantly affect the effective stiffness/strength. In particular, while in-plane moduli decreased with increasing density and depth, thickness-directional moduli and poisson ratios tended to increase; thus, it was demonstrated that needle punching parameters are an effective design tool for adjusting through-thickness stiffness and anisotropy [58]. Furthermore, needle-punched oxidized polyacrylonitrile (PAN)-based nonwoven carbon felts have been used to fabricate C/Ph composites by varying the needling density, followed by carbonization and phenolic impregnation. Tensile, flexural, and short-beam tests indicate that strength increases up to an optimum needling density but decreases beyond it due to fibre-network damage. Torch results show an increased insulation index with needling density, little change in linear erosion rate, and higher through-thickness thermal conductivity, underscoring the need for an optimal needling window for C/Ph ablators [58]. In addition to these studies, as the needle punching parameters (depth, pin number, and interlayer density) increase, the stiffness shifts from the in-plane to the thickness direction: Young's modulus in longitudinal direction (E_1) decreases while Young's modulus in through-thickness direction (E_3) increases; conversely, shear moduli (especially G_{12} and G_{23}) generally show a decreasing trend. Therefore, while needle punching is an effective design tool that "increases z-direction stiffness," it requires an optimum parameter window in terms of in-plane stiffness/shear [61]. Needled C/C composites with nonwoven cloth layers arranged at 0°/90° and ±45°, together with an interleaved short-fiber felt, have been evaluated under compressive loading at temperatures up to 2800 °C. The reported observations indicate that

cracking preferentially initiates within the needled regions where needling holes and local fiber disturbance are present and that the overall damage severity increases with temperature. In particular, fiber breakage in the ±45° layers and progressive delamination and plastic buckling under compression become more pronounced at elevated temperatures, highlighting the needled zone as the primary damage initiation and growth region [62]. In addition, a thermal reaction based mesoscale ablation model has been proposed to capture how needle-punched architectures influence phase degradation and pyrolysis. Using an representative volume element (RVE) representation of a phenolic matrix containing 0°/90° unidirectional (UD) carbon-fiber bundles and a short-fiber felt layer, the study shows that the needle pattern induces a distinctly non-uniform temperature field compared with homogeneous models. Owing to the higher axial thermal conductivity of carbon bundles, locally elevated temperatures and steeper gradients develop in bundle-rich regions, which can accelerate pyrolysis and alter the overall heat-transfer and ablation response [63]. As a more recent contribution, nanoparticulate phenolic composites reinforced with needle-punched carbon/quartz preforms have been reported to simultaneously achieve low thermal conductivity, high tensile strength, enhanced ablation resistance, and low density, indicating their strong potential for lightweight TPS applications [64]. In addition, the effect of fibre/fabric orientation on the performance of needle-punched phenolic composites has been highlighted, showing that the anisotropic microstructure leads to direction-dependent mechanical and thermal responses. Specimens evaluated along the 0° (XY), 90° (Z), and 45° directions exhibited distinct behaviors: the 0° direction provided the highest tensile strength, the 45° direction yielded the highest compressive strength but indicated weaker interlayer bonding at low strain, and heat-transfer analyses suggested that the 0°oriented stacked fabrics offer the most effective thermal insulation. Overall, the results demonstrate that the placement angle of the textile reinforcement is a key design variable governing both load-bearing capacity and ablation/insulation performance [65]. In addition, the role of weave pattern in needle-punched preform reinforced nanoporous phenolic composites has been highlighted. Under comparable preform densities, plain weave generally provides the most favorable tensile response, whereas twill and satin weaves exhibit distinct tensile behaviors due to differences in crossover density and yarn crimp. Overall, the results indicate that the woven-fabric architecture is the primary load-bearing contributor, making weave selection a key design variable in needle-punched composites [66]. In

addition, the stacking sequence of woven plies and needle-punched felt interleaves was reported to markedly improve interlaminar shear strength (ILSS) and impact damage tolerance. Needle-punched with interleaves placed between fabric layers exhibited higher shear load-carrying capacity and a more stable post-impact response, indicating stronger through-thickness load transfer and a clear reduction in delamination propensity. Overall, the results emphasize that fabric–felt placement is a primary design variable for controlling interlayer integrity [67].

In addition to , several studies have reported ablation rates for silica/phenolic systems in both laminated and needle-punched configurations to directly relate material selection and textile architecture to ablation performance. A combined theoretical and experimental investigation on silica fiber–reinforced phenolic composites reported a linear ablation rate on the order of about 0.2 mm/s under ablative conditions [68]. Moreover, 2.5D needle-punched silica fabric–felt/phenolic composites with different configurations were shown to deliver notably lower recession, with torch tests indicating a linear ablation rate of about 0.05 mm/s and a mass ablation rate of about 0.04 g/s . In addition to the ablative response, mechanical characterization confirmed that needle-punching significantly enhanced structural integrity.The needle-punched composites demonstrated an approximately 181% increase in flexural strength, a 27% increase in interlaminar shear strength, and a about 2% increase in tensile strength relative to the baseline configuration [69]. According to the literature, silica fiber reinforced phenolic composites have great thermal stability overall, and surface recession can be further suppressed while still providing effective thermal protection by adding through-thickness reinforcement by needle punching.

The results of these studies encourage the use of silica fabric-felt architectures produced by needle punching as a practical way to increase delamination resistance and improve ablative efficiency, and provide a clear basis for the experimental framework adopted in the present study.

1.2.5 Manufacturing techniques

Maintaining the geometric form and structural integrity of the nozzle and throat area throughout combustion under abrasive operating conditions is critical for a rocket engine to reliably, repeatedly, and predictably convert exhaust gas energy into thrust. Therefore, not only the composition of the material to be used in these regions but also

its microstructure, oriented reinforcement architecture, porosity/delamination tendency, and erosion-ablation behavior, as well as the manufacturing method, should be considered as fundamental design parameters that directly determine performance. Choosing the most suitable production method involves minimizing these defects to obtain a high-quality final product while simultaneously optimizing production costs. However, in practice, processes that deliver high quality and repeatability are often more expensive, particularly in terms of molding/tooling and production costs. Composites which are continuous fiber composites, chopped fiber composites, woven fiber composites, and hybrid composites can be manufactured using different manufacturing processes. Therefore, fiber type directly affects the feasibility and efficiency of the process to be selected. The Figure 1.22 shows the manufacturing techniques according to the fiber type [70].

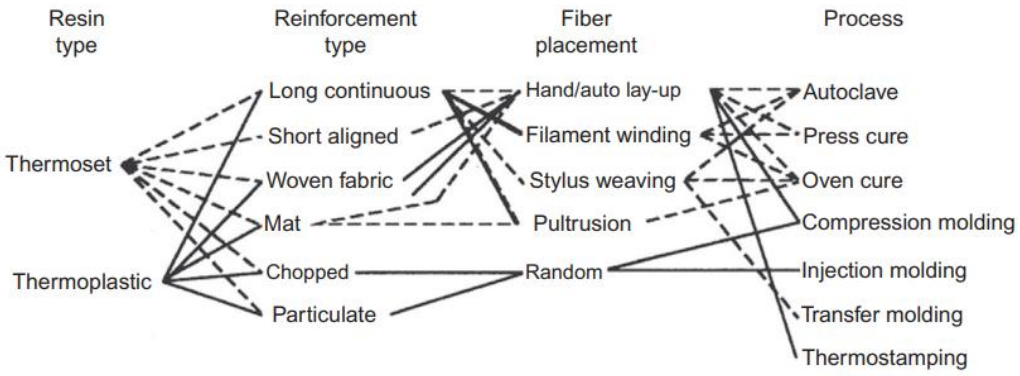

Figure 1.22 : Composite constituent materials and manufacturing alternatives [70].

While hand lay-up was common in the early stages of composite production, increasing scale and quality requirements in the aerospace industry have accelerated the development of more controlled, repeatable, and high-productivity methods. In this context filament winding, compression molding, resin transfer molding (RTM), vacuum-assisted resin transfer molding (VARTM), and pultrusion are the main manufacturing techniques that stand out as alternatives to the traditional hand lay-up approach [70].

The hand lay-up method is one of the more traditional composite manufacturing techniques that has been used for a long time in the industry. In this method plies are prepared completely by wetting with resin, and they are layered on top of each other until the desired thickness is reached. Although the method is generally reliable and easy to implement, it requires intensive labor and a long production time; furthermore,

the final product quality depends largely on operator skill, and production capacity may be limited with complex geometries. Different types of fibers, such as carbon or glass, are suitable for this method in various forms including continuous/chopped fibers, woven fabrics, etc. The spray lay-up method relies on spraying resin and chopped fibers onto the mold surface using a handgun. It is preferred because it requires low-cost molds and is suitable for the production of large-sized parts [70].

RTM technique is suitable for medium-volume production; the production speed is neither too low nor too high. In the process, fiber reinforcement (matte/fabric) is placed at the bottom of the mold, and after the mold is closed, the matrix resin is injected, usually at low pressure (mostly <100 psi), until the mold is completely filled. The ability to manufacture complex geometries at relatively high production speeds and to obtain products close to autoclave quality when proper process control is ensured are important advantages of RTM. In addition to RTM can offer a cost advantage compared to compression molding in some cases. Polyester, acrylic, epoxy, phenolic, and vinyl ester are commonly used as matrices; and fabric, strand mat, unidirectional fiber, or woven roving are commonly used as reinforcement. Another technique is compression molding, one of the oldest methods, which is based on compressing the material between two steel molds under heat and high pressure, and is widely used in composite part production. While the method is suitable for producing parts of different sizes, tooling costs can be high in low-volume production. Injection molding is a method that allows for high production speeds, complex geometries, and high-volume production with low labor costs. As shown in the Figure 1.23, molten polymer (thermoset/thermoplastic) and usually chopped fibers are liquefied in a heated cylinder using a chamber-screw system and injected into the mold under pressure; after the material cures/solidifies in the mold, the part is removed from the mold [70].

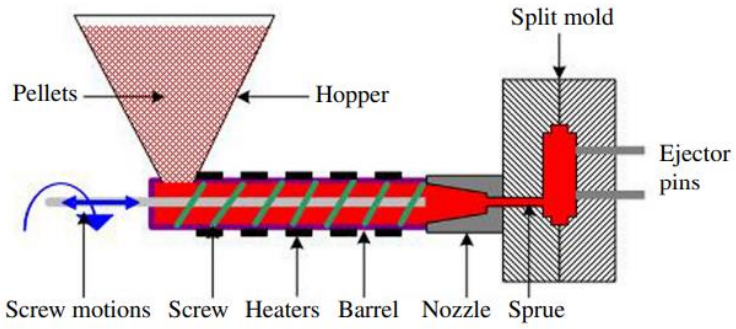

Figure 1.23 : Injection molding [70].

VARTM is an advanced variant of hand lay-up that allows mechanical pressure to be applied to the laminate during curing. Prepreg layers are laid in the mold in the desired arrangement; a release film, absorbent (breather/bleeder) layers, and a vacuum bag are used to seal them. The vacuum removes trapped air and excess resin, reducing voids and improving interlayer adhesion/compaction as shown in Figure 1.24. Epoxy, polyamide, and phenolic matrices are commonly used in this method, and it has been reported that appropriate vacuum pressure has a significant effect on tensile strength and modulus [70].

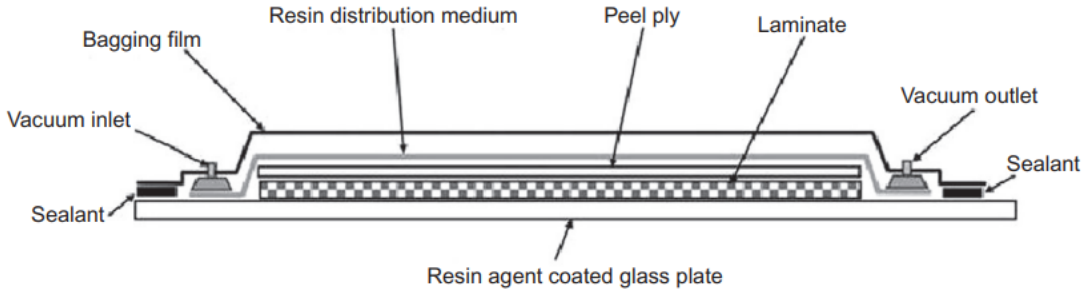

Figure 1.24 : VARTM manufacturing technique [70].

Autoclaving is a widely used manufacturing method in aerospace applications. Prepreg layers are laid in molds, vacuum-bagged, and then cured in an autoclave at high temperatures and approximately 50–100 psi pressure; this results in denser and less void composites. However, the process is lengthy, operator-skill dependent, and relatively high in terms of labor/production costs. Pultrusion is a continuous production method in which continuous bundles of fibers are shaped by being passed through a resin bath and pulled through a die, usually cured within the die as shown in the Figure 1.25. The die cross-section determines the product form; high strength is achieved thanks to a high fiber volume ratio, and labor requirements are low. Thermosets are mostly used as matrices; phenolics stand out due to their high temperature resistance and cost advantage, while polyester/vinyl ester/epoxy are also common [70].

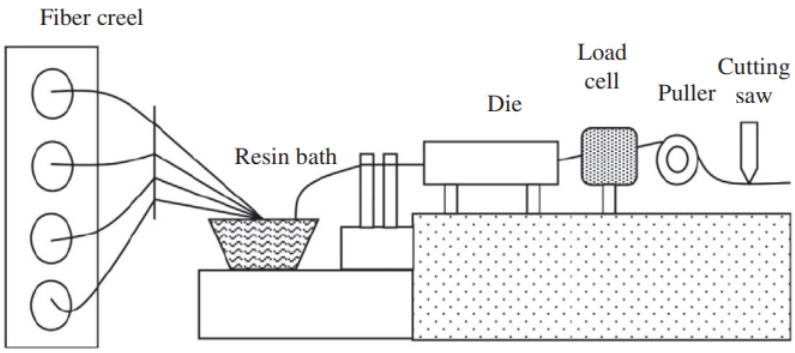

Figure 1.25 : Pultrusion manufacturing technique [70].

Filament winding is an established method for producing composite parts, particularly symmetrical and circular, by controlled winding of resin-impregnated continuous fibers onto a rotating mandrel as shown in Figure 1.26. Similar to pultrusion, the fibers are passed through a resin bath and distributed homogeneously along the mandrel during winding; a high fiber volume ratio can be achieved. Thermoset matrices and roving/stand fibers are commonly used; applications include parts such as pipes, pressure vessels, and tanks [70].

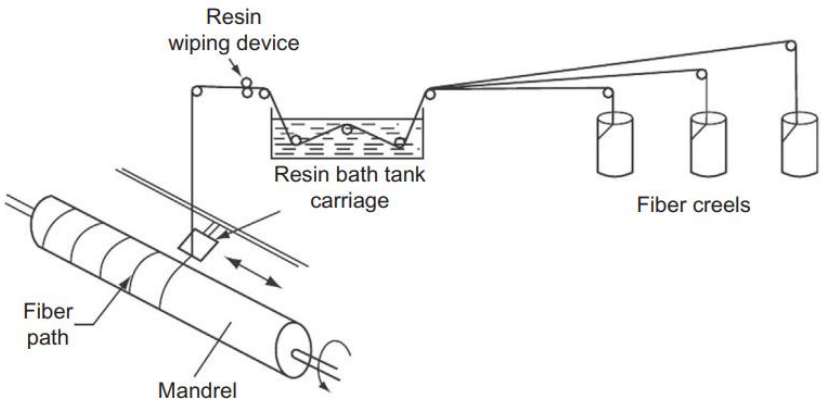

Figure 1.26 : Diagram of the filament winding manufacturing [70].

Each composite manufacturing method presents different advantages and limitations depending on parameters such as the form of the reinforcing fiber (continuous/chopped, woven/UD), matrix type, target fiber volume ratio, and expected structural performance. Phenolic resins, particularly preferred in high-temperature environments, are an important option in polymer-based composites due to their thermal stability and contribution to ablation behavior; however, they are a matrix with a narrow process window and relatively difficult to produce due to factors such as high viscosity, volatile/by-product formation and gas release (outgassing) during curing,

shrinkage, and susceptibility to crack/void formation [71]. Therefore, the production method should be selected considering the curing kinetics and volatile matter management of the phenolic resin, along with the service temperature requirements; the temperature-pressure-time parameters should be meticulously optimized to control porosity and interlayer adhesion. Indeed, the literature contains extensive studies examining the effects of different manufacturing approaches (e.g., RTM/VARTM, compression molding, autoclaving, etc.) on process outputs and final performance of phenolic-based composites. Within the scope of RTM, porosity formation during the curing of phenolic resin was investigated; it was reported that porosity became particularly pronounced after gelation and that degassing applied at the beginning of curing reduced porosity [72]. It has been reported that carbon-phenolic laminates for rocket engine applications can be produced by non-autoclave infusion; the quality/mechanical performance of the produced samples was evaluated and their thermomechanical behavior was investigated with oxy-acetylene torch ablation tests [73]. Carbon fiber reinforced phenolic composites were produced using hot compression molding with varying SiC filler ratios (0–5 wt.%), and their thermal/ablation and mechanical performances were evaluated for TPS applications. The results showed that 3% SiC addition provided the most significant improvement, and the SiO_2 layer formed on the surface after ablation was related to the protective effect [74]. Vacuum infusion of phenolic resin into dry textile preforms offers simpler tooling setup and more practical process control compared to closed mold/autoclave-based methods; while vacuum-assisted flow allows for more homogeneous wetting and lower porosity [75].

1.3 Hypothesis

This thesis hypothesizes that a silica fabric–silica felt architecture produced by the needle punching method will enhance interlayer load transfer in laminated high-silica/phenolic ablative composites by creating fiber bridging in the thickness direction (z-direction). This structural bonding is expected to reduce the effect of internal pressures and interfacial stresses that develop as a result of the z-direction transport of gases formed by matrix pyrolysis during ablation. Thus, it is predicted that layer-by-layer separation will be suppressed, delamination will be limited, and interlaminar shear strength will be increased.

It is also thought that the fabric-felt stacking arrangement will improve the continuity and stability of the char layer by regulating the porosity/transport pathways. This is expected to reduce surface regression, thereby lowering the linear ablation rate and total material loss. On the other hand, since needling can cause local disruptions in the in-plane fiber network, limited losses in tensile and flexural strength may be observed. However, it is assumed that these losses can be kept at an acceptable level with an appropriate fabric/felt ratio, stacking order, and fiber volume ratio, thus achieving an optimum balance between ablation performance and mechanical integrity.

2. MATERIALS AND METHODS

In this thesis, a reference laminated composite consisting solely of high-silica fabric layers was first produced. Subsequently, composite samples were fabricated from silica fabric-silica felt architectures with different fabric/felt arrangements using the needle punching method. An extra configuration with the same fabric-felt components but no needling was created and included to the comparison group in order to better illustrate the impact of the needling technique on interlayer integrity and delamination behavior. Tensile, three-point bending, and short beam shear tests were performed to quantitatively determine the mechanical behavior of all generated configurations. Ablation performance was next assessed using oxy-propan torch tests; mass ablation rate and linear ablation rate were computed from the measured data, and the structures' comparative ablation behavior was examined.

2.1 Materials

In this study, a woven fabric structure was chosen as the reinforcement phase in the production of composite materials. The reinforcement material used is a fabric with an 8H satin (8-harness satin) weave pattern made from high silica fibers coated with a thin vermiculite-based finish for enhanced thermal protection and supplied by Valmiera Glass Group, Latvia. The basic physical and structural properties of the high silica fabric are presented in Table 2.1.

Table 2.1 : The basic physical and structural properties of the high silica fabric.

Thickness (mm)	Mass per unit area (g/m^2)	Tensile strength (N/5cm)	Content of main components
0.78 ± 0.07	600 ± 30	warp:2800 weft: 1900	SiO_2:95±1% Al_2O_3:3.5±0.5%

In satin weave, the warp and weft yarns are bonded at specific intervals, resulting in relatively long floats on the surface. In 8H satin, the bonding points are less densely distributed, allowing the threads to move freely over longer distances on the fabric

surface. This results in a smoother surface and lower crimp (yarn waviness) characteristics. As seen in Figure 2.1a, the warp face is dominated by warp yarn flocs, creating a more continuous appearance on the surface; while on the weft face in Figure 2.1b, the weft yarn flocs become more prominent and the distribution of bonding points creates a different surface texture.

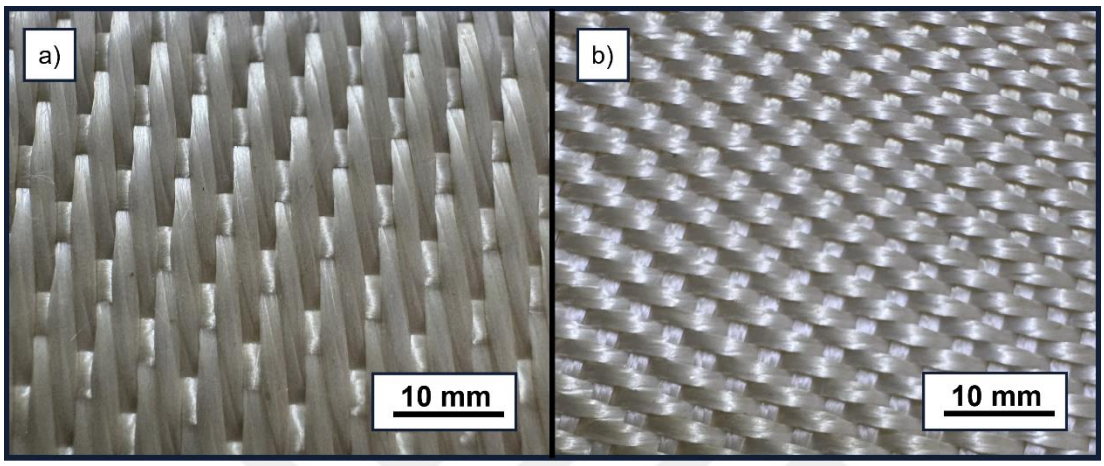

Figure 2.1 : Surface views of 8H satin high silica fabric: (a) front side (warp side), (b) back side (weft side).

This surface asymmetry can influence the local void/channel geometry of the fabric and resin flow paths, playing a role in the formation of resin-rich regions and interlayer contact/adhesion during impregnation. In this study, an 8-harness satin (8H) architecture was selected because its longer float lengths and lower crimp provide a smoother, more continuous surface and a less constrained yarn path, which are expected to facilitate both impregnation and through-thickness reinforcement. Furthermore, the dominance of warp floats on the front (warp) surface allowed needles to penetrate the fabric more stably and with lower resistance during needle punching. This resulted in easier transport of short fibers of the silica felt into the woven structure by the needles, and increased fiber transfer/anchoring, particularly along the float regions in the warp direction. In contrast, the back (weft) surface, due to its different bonding distribution, offered a more limited path for needle penetration and fiber transfer.

After determining the weaving architecture and surface characteristics of 8H satin fabric, the next step involved investigating the yarn form of the high-silica fibers that constitute the reinforcement, and in particular, the effect of the yarn structure (fiber bundle, twist/filament arrangement, etc.) on the fabric's internal behavior was

investigated in detail. Experimental studies aimed at determining the physical and mechanical behavior of the yarn used in this study were carried out at the Physics Laboratory of the Faculty of Textile Technologies, Istanbul Technical University.

High-silica yarns extracted from the fabric were placed in a twisting device, as shown in the Figure 2.2, to determine the amount of twist in the yarn and to evaluate its physical structure.

Figure 2.2 : Yarn twist tester.

Measurements revealed that the yarn's twist rate was 23 t/m. Following the measurement, the twisted structure of the yarn was examined; it was observed that the silica yarn exhibited a plied yarn character, formed by twisting multiple single yarns together as shown in the Figure 2.3. This plied structure was determined to be formed by the twisting together of single yarns consisting of short staple fibers.

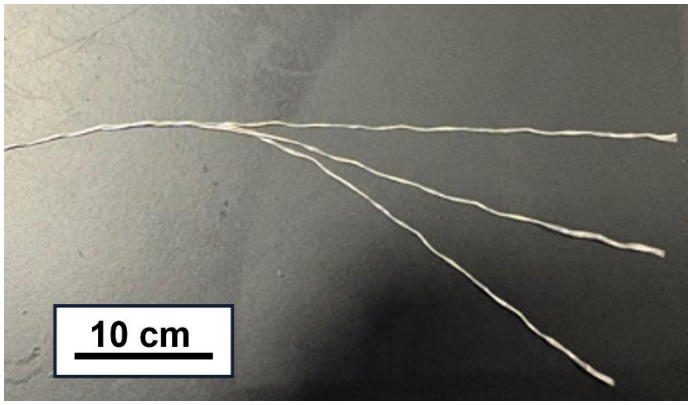

Figure 2.3 : Appearance of the plied silica yarn showing three-ply structure.

Single-yarn tensile tests were performed according to ASTM D2256 at a crosshead speed of 250 mm/min. Five specimens were tested to characterize the mechanical behavior of the vermiculite-coated silica yarns as shown in the Figure 2.4. The coated yarns exhibited an average tensile strength of 218.034 ± 37.014 MPa and an average elastic modulus of 7.442 ± 0.732 GPa.

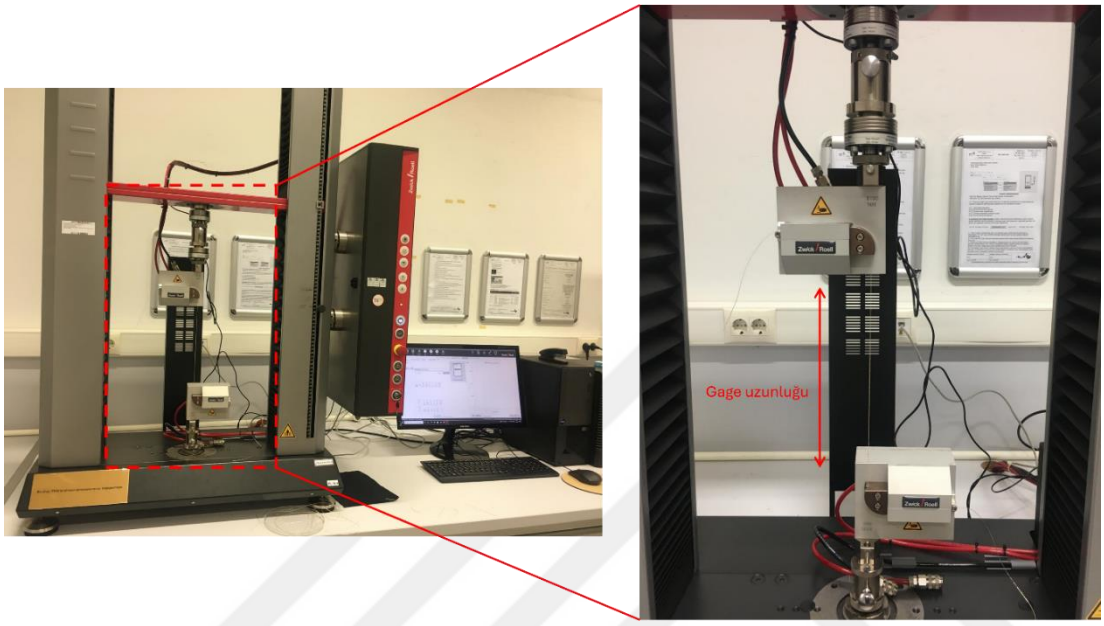

Figure 2.4 : Universal Testing Machine (UTM) used for single-yarn tensile tests (ASTM D2256).

In addition to, a silica needle felt was used as the interlayer material in this study. The basic physical and structural properties of the silica felt are presented in Table 2.2.

Table 2.2 : The basic physical and structural properties of the silica felt.

Thickness (mm)	Mass per unit area (g/m^2)	Tensile strength (N/50*200mm)	Content of main components	Density (kg/ m^3)
5 ± 0.05	650 ± 0.05	warp:20 weft: 50	SiO_2:96±1%	130± 0.05

In this study, silica felt, used as an interlayer material, has a nonwoven structure and is primarily formed by the random arrangement of short staple silica fibers as shown inn the Figure 2.5. The structure that holds these fibers together is achieved through a needle punching process applied during production; by carrying the fibers along the thickness with barbed needles, mechanical interlocking is created between the fibers, resulting in a nonwoven felt layer.

Figure 2.5 : Structure of silica felt.

The primary rationale for choosing silica felt in this thesis is to transfer the randomly oriented short fibers in the felt into the structure of the woven silica fabric using hooked needles during needle punching, and to create a locking/anchoring effect by forming fiber bridging between the fabric layers. Thus, the aim is to increase interlayer mechanical bonding by transferring short fibers originating from the interlayer into the woven structure and to improve delamination resistance, especially in the thickness direction (Z-direction).

A resol-type phenolic resin, supplied by Çukurova Kimya (Türkiye), was used as the matrix material in the composite manufacturing. Since volatile components are removed, water is released (condensation) and consequently gas is released/air bubbles form during the curing of phenolic resins as shown in the Figure 2.6, knowing the thermal behavior of the resin before production is critically important for determining the temperature-pressure profile and holding stages to be applied.

Figure 2.6 : Porosity in phenolic resin caused by gas release during curing.

For this purpose, thermogravimetric analysis (TGA) was applied to the resin. TGA measurements were performed in a 50 mL/min nitrogen (N_2) atmosphere as shown in the Figure 2.7, and the char yield of the resol resin was determined to be in the range

of 60–61%. The measurement was continued up to 900 °C; no isothermal holding was performed at 900 °C. This high char yield is consistent with the tendency of phenolic resins to form carbonaceous residues after pyrolysis, and indicates the potential of the matrix to contribute to structural integrity at high temperatures in thermal protection applications.

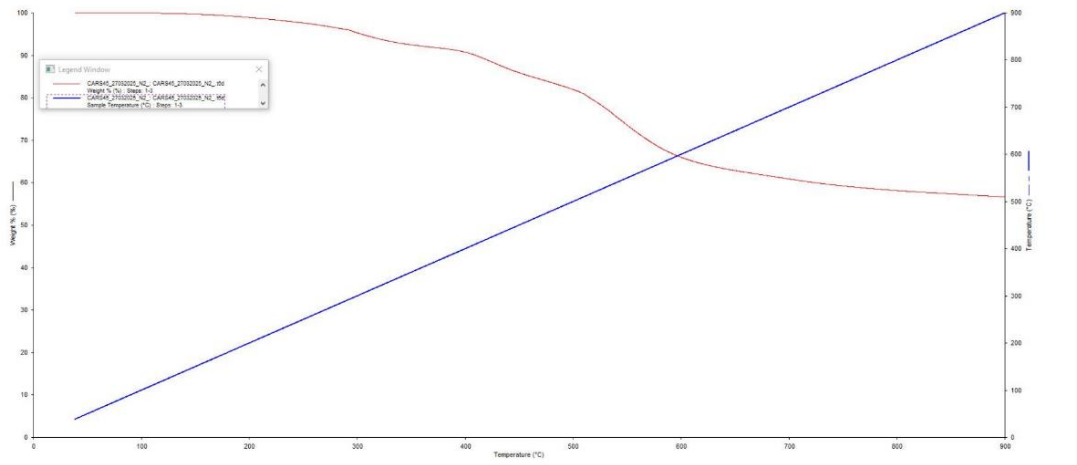

Figure 2.7 : Thermogravimetric analysis (TGA) curve of the resol-type phenolic resin under nitrogen atmosphere.

The TGA curve shows that the resin exhibits limited mass loss at low temperatures (approximately 25–150/200 °C), while mass loss increases significantly in the range of approximately 250–650 °C. In terms of the production cycle, the first range, in particular, was used as a reference for the volatile degassing step before impregnation/curing of the resin; the rapid mass loss region at high temperatures indicates thermal decomposition and intense gas release behavior of the phenolic structure, suggesting that production temperatures should be kept away from this region.

In addition to TGA, differential scanning calorimetry (DSC) was conducted to identify the main thermal events associated with the curing reaction of the resol phenolic resin and to support the selection of the curing schedule. As shown in Figure 2.8, the resin exhibits a pronounced exothermic curing peak with a peak temperature of approximately 178.2 °C, while the onset of the exothermic reaction starts at about 166.5 °C. The normalized reaction enthalpy was measured as approximately 220 J/g.

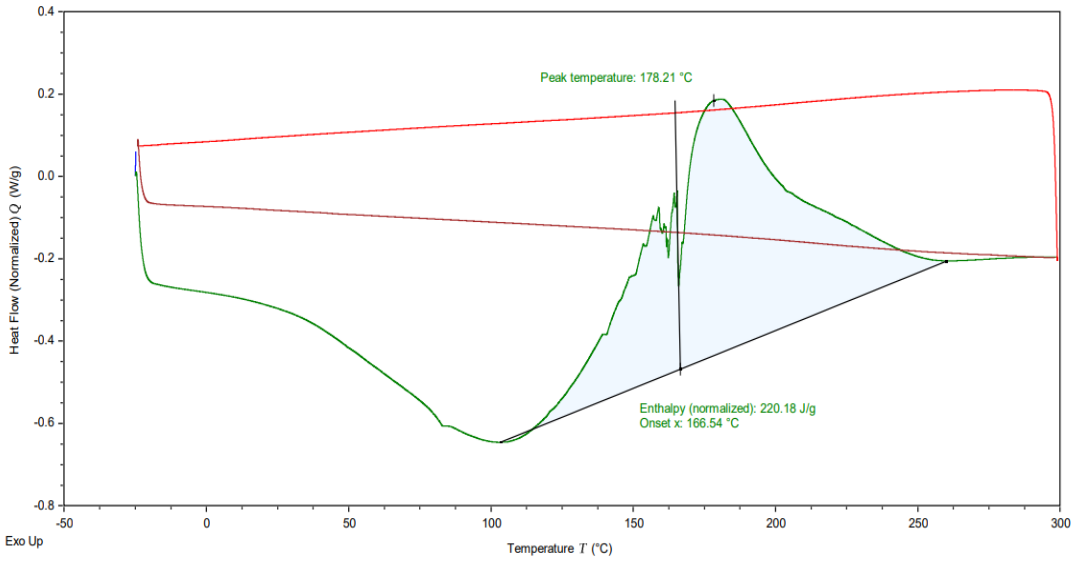

Figure 2.8 : DSC thermogram of the resol-type phenolic resin showing the curing exotherm.

These DSC results indicate that significant crosslinking occurs in the about 165–200 °C range, which is consistent with applying the final curing stage near the upper end of this interval to ensure completion of cure. Moreover, the onset temperature provides a practical reference for defining the transition from degassing/flow-dominated stages to cure-dominated stages in the temperature–pressure profile, helping to minimize void formation during processing.

2.2 Laminate Composite Fabrication

In this study, reference (conventional) laminated composite samples were also produced in order to compare the performance of structures reinforced with needle punching. The laminate composite samples were manufactured using an 8H HSF fabric and a resol-type phenolic resin with in-plane dimensions of 27 x 27 cm. The laminate preforms were prepared by stacking 18 fabric plies in a controlled lay-up sequence, where the warp-face side of each ply was oriented consistently so that the warp faces were aligned on the same side throughout the stack. This controlled ply orientation was selected to ensure repeatable surface topology and yarn-float distribution across interfaces, thereby improving lay-up consistency and enabling a more reliable comparison of impregnation and consolidation behavior in the reference laminates.

The HSF textiles were first impregnated with preheated phenolic resin using the VARTM technique, as shown in Figure 2.9. To increase resin-flow stability, heat was given to the preform from about 30 to 40 cm during impregnation. The impregnated preforms were then subjected to hot pressing for curing and consolidation processes. During the curing cycle, the temperature was gradually increased, taking into account the volatile/water release and gel formation behavior of the phenolic resin. Specifically, the temperature was started at 70 °C, then increased using intermediate stages; longer holding periods were applied at 130 °C, and the cycle was completed by raising the temperature to approximately 200 °C. Temperature values were monitored in real-time throughout the process using thermocouples placed inside the laminate.

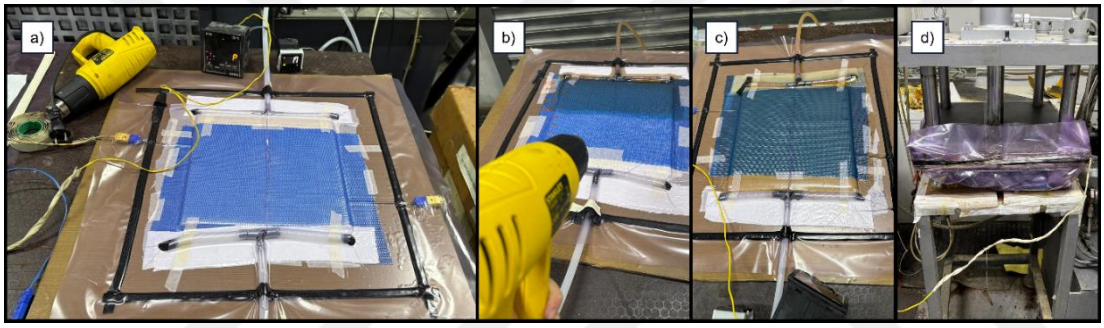

Figure 2.9 : Production process of HSF–phenolic composites; (a–c) infusion process and superficial heating steps with VARTM method, (d) curing process under hot-press.

The pressing process was carried out using a two-stage temperature-pressure profile. In the first stage, the sample was pressed at 114 °C under 100 bar pressure; after approximately half an hour, the temperature was increased to 116 °C and a second pressing was applied under the same 100 bar pressure. The aim of this approach was to limit porosity and achieve the targeted fiber volume fraction by ensuring proper consolidation before the resin fully gels and loses its flowability. Since a fiber volume fraction of approximately 60% was targeted for the reference laminates in this study, the pressing timing and gradual temperature increase were adjusted considering the curing kinetics of the phenolic resin.

The resultant laminate showed a consistent thickness of 8.27 mm following hot-press consolidation, which correlated to a measured fiber volume fraction of 66.7%. In addition to offering a representative reference configuration for comparison with the

needle-punched composite counterparts, these specifications were chosen to provide sufficient structural integrity.

2.3 Needle-Punched Composie Production

Preforms with various fabric/felt ratios were produced using a custom-designed needle-punching machine developed specifically for this study in Figure 2.10 to fabricate the needle-punched composite specimens. The system consists of a needle board carrying an array of barbed (triangular-notched) needles, which was rigidly mounted to a piston/actuator and driven in a controlled reciprocating (up–down) motion.

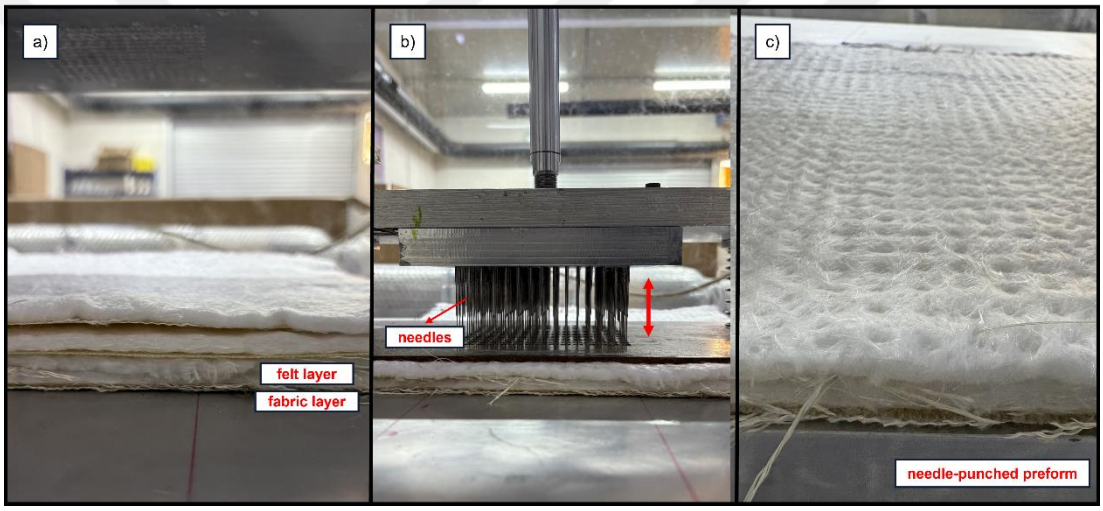

Figure 2.10 : Needle-punching process and resulting preform:(a)) Initial stacking of silica felt on the 8H satin-weave HSF fabric; (b) Up–down movement of barbed needles during needling;(c) Through-thickness fiber entanglement formed after needle punching.

During operation, the preform stack was positioned on a flat support table and aligned beneath the needle board. A 10 x 10 cm needle plate with 225 barbed needles or a needle density of 2.25 needles/cm² inside the active needling zone was used for the needle-punch procedure. To ensure consistent exposure, this plate was repeatedly passed over the whole 27 × 27 cm preform throughout processing. The effective needling intensity applied to the preforms was roughly 90–113 strokes/cm², and this intensity was maintained constant across all needle-punched configurations, taking into account the needling frequency (1 stroke/s) and the repeated penetration at each place (40–50 strokes).

The needle-punching process was conducted in a layer-by-layer lay-up sequence. First, the HSF woven fabric layer was placed on the support surface. Next, a silica needle-felt layer was positioned on top of the fabric, and the stacked assembly was subjected to needle punching. As the needle board penetrates the stack, the barbs on the needles mechanically capture short staple silica fibers from the felt and transport them through the thickness into and across the woven fabric architecture. Upon needle withdrawal, a portion of these fibers remains anchored within the yarn interstices and pore channels of the woven layer, producing mechanical interlocking between adjacent layers. This repeated penetration-withdrawal cycle promotes the formation of through-thickness (Z-direction) fiber bridging, where transferred felt fibers act as micro-reinforcements connecting neighboring plies and restricting relative sliding at the interfaces. Consequently, the initially 2D laminate architecture is converted into a 2.5D fiber network, enhancing interlaminar load transfer and improving structural integrity by increasing resistance to interlayer separation (delamination). Using the same process route, preforms with different fabric/felt stacking configurations were manufactured to systematically evaluate the effect of the reinforcement architecture on composite performance.

Preforms with different fiber arrangements were created using this process in order to further examine the impacts of needle-punching on delamination resistance and ablation behavior. Table 2.3 provides a summary of the structural configurations and parameters of the needle-punched preforms.

Table 2.3 : Needle-punched preforms with different configurations.

Specimen ID	Number of Fabric Layer	Number of Felt Layer	Total Layer
NP-1/1	6	6	12
NP-2/1	8	4	12
NP-3/1	9	3	12

For all needle-punched configurations, the total preform thickness was standardized to 12 layers to provide a consistent basis for comparing different fabric-felt architectures and to minimize thickness-related bias. As illustrated in Figure 2.11, the NP notation describes the fabric-to-felt stacking unit: NP-1/1 denotes a repeating sequence of 1 fabric layer + 1 felt layer, NP-2/1 denotes 2 fabric layers + 1 felt layer, and NP-3/1 denotes 3 fabric layers + 1 felt layer. Each stacking unit was repeated as required so that the final preform contained 12 layers in total, ensuring manufacturing consistency

across specimens. Three different configurations were chosen to gradually increase the fabric ratio while keeping the total number of layers constant. This allowed for a clear comparison of how effective needle punching is at creating fiber bridges in the Z-direction as the fabric quantity increases, and how this affects the mechanical and ablation behavior of the composite. Furthermore, when comparing NP samples with the reference HSF laminate, care was taken to keep the fiber volume fraction as similar as possible; because the reference composite consisted of 18 layers of fabric, while the NP samples contained felt layers, it was necessary to adapt the stacking strategy in order to approximate a similar reinforcement content.

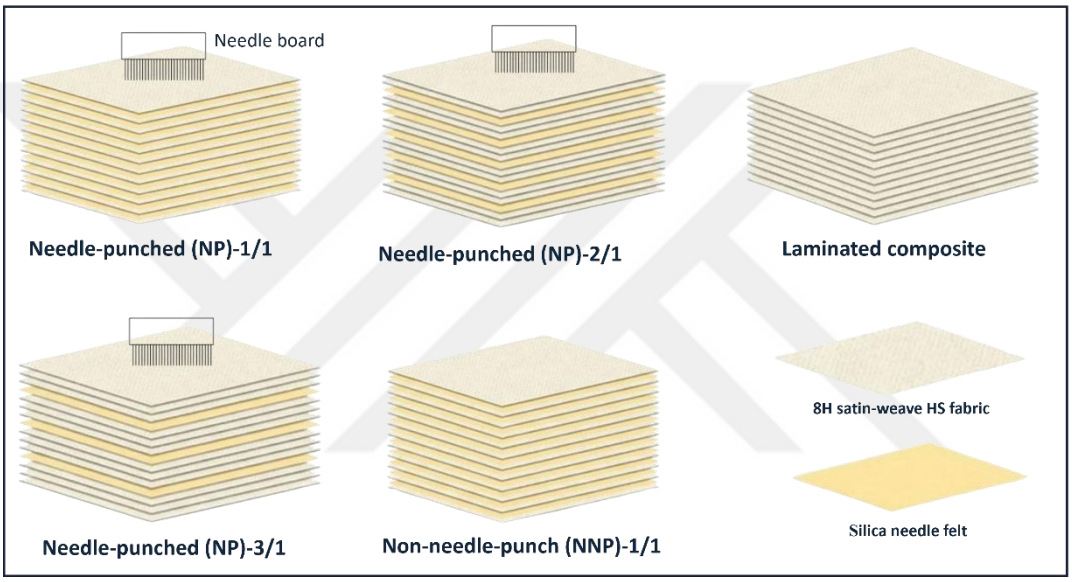

Figure 2.11 : Schematic of stacking configurations for NP, NNP, and reference laminates.

The preforms were transformed into composites using the same manufacturing method as the baseline HSF laminate depicted in Figure 2.9 after the needle-punch process. Resol-type phenolic resin was first impregnated into the needle-punched preforms using the VARTM process. The resin-impregnated constructions were then moved to the hot press. The reference laminate curing cycle was not suitable for the needle-punched samples; the felt layer increased thermal insulation, reduced heat penetration, and led to incomplete curing. Therefore, in NP composites, the curing cycle has been redesigned by dividing it into more stages to ensure more homogeneous heating and safe completion of the resin-to-gel curing transition. The process was started at 70 °C; the temperature was gradually increased by applying specific holding times at intermediate temperature stages, and the cycle was completed by raising the

temperature to 205 °C and holding it for a total of 6 hours. Thanks to this gradual temperature approach, curing was achieved in NP samples and temperature gradients were reduced throughout the thickness. In pressure management, a pressure of 50 bar was applied in the first step of the production process, followed by a second compression at the same pressure value in the third step. No further pressure increases were made after this stage; however, during any potential pressure drops throughout the process, the system automatically restored the pressure to its previous level, maintaining stability. This controlled pressure application helped ensure sufficient consolidation before the resin fully gelled; consequently, the final thickness of the sample and the targeted fiber volume ratio were achieved. As a result, pinpoint marks and a homogeneous resin impregnation appearance, as well as a homogeneous temperature distribution, were observed on the surface as shown in the Figure 2.12.

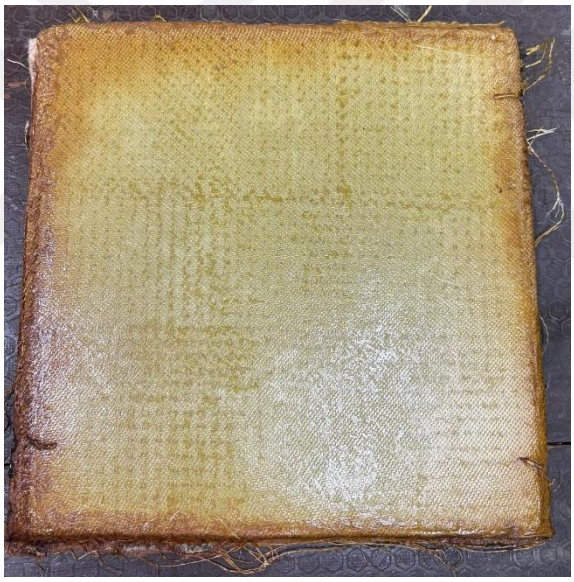

Figure 2.12 : Fully cured needle-punched composite plate obtained after stepwise curing profiling.

Following consolidation, all configurations' ultimate thicknesses and associated fiber volume fractions were calculated; the outcomes are compiled in Table 2.4 below.

Table 2.4 : Thickness and fiber volume fraction measurements of the needle-punched composite.

Specimen ID	Thickness ($\boldsymbol{mm}$)	Fiber Volume Fraction $\boldsymbol{V_f}$ (%)
NP-1/1	9	60
NP-2/1	7.5	65.7
NP-3/1	8	63.3

In needle-punched samples, final fiber volume ratio values were obtained in the range of 60–65.7%; these results indicate that consolidation close to the targeted approximately 60% V_f level was achieved, and suitable for comparison between configurations. Furthermore, the final thickness of the needle-punched composite samples ranged from 7.5 to 9.0 mm.

2.4 Non-Needle-Punch Composite Preparation

To more clearly observe delamination behavior, an additional composite configuration consisting of silica fabric and silica felt was also manufactured in this study. So that this configuration represents a reference preform structure created solely by stacking layers of silica fabric and silica felt without the application of needle punching. In order to more accurately compare the effect of the NP-1/1, the silica-felt configuration was designed to maintain the 1-layer fabric + 1-layer felt arrangement; the production method was kept the same as the other samples, and care was taken to ensure that the sample's overall thickness and fiber volume fraction were as similar as possible to the other configurations. Table 2.5 provides a summary of the material parameters used for this reference structure.

Table 2.5 : The material parameters of the non-needle-punched composite.

Specimen ID	Number of Fabric Layer	Number of Felt Layer	Total Layer	Thickness (mm)	Fiber Volume Fraction V_f (%)
NNP-1/1	6	6	12	8.99	57.47

2.5 Characterization Methods

This section summarizes the methods used to evaluate the mechanical and ablation responses of the needle-punched composites and the reference laminate. The reference laminate was characterized by tensile, short-beam shear, and three-point bending tests to establish its mechanical behavior. The same tests were applied to the needle-punched specimens to quantify the effect of needle-induced interlayer locking and Z-direction fiber bridging on through-thickness integrity and delamination resistance. In addition, torch tests were conducted using a custom-built setup to measure mass loss, linear ablation rate, and overall ablation performance. The results were then compared

across configurations to determine how the needle-punch architecture influences delamination and ablation behavior.

2.5.1 Mechanical characterization

In the first stage, tensile tests were performed to quantify the axial strength of the reference laminate and the different NP configurations and to capture the effect of NP-induced disturbance in the woven architecture. Flexural performance was evaluated by three-point bending, while short-beam shear tests were used to determine interlaminar shear strength (ILSS) and infer delamination resistance for both baseline and NP specimens. The observed damage modes were then analyzed to relate the mechanical response to NP-driven through-thickness (z-direction) fibre bridging.

2.5.1.1 Tensile test

The ASTM D638 standard was followed in the tensile testing of the reference laminate and the needle-punched composites with various configurations. The specimens' failure modes, deformation behavior, and tensile strength were assessed. A Vector universal testing machine with a gauge length of 115 mm was used to test each sample. As seen in Figure 2.13, the tests were carried out at a constant crosshead displacement rate of 2 mm/min.

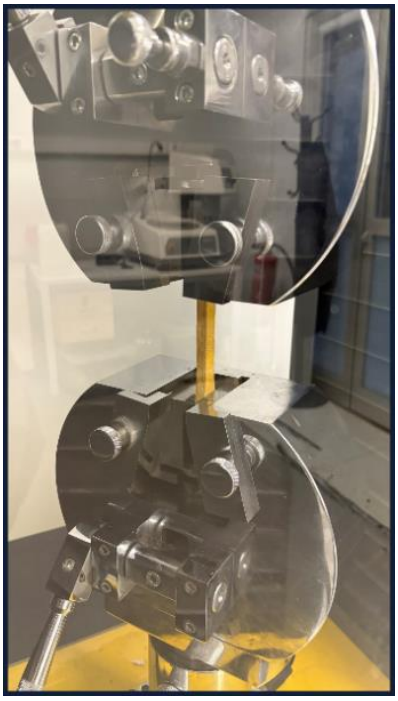

Figure 2.13 : Tensile testing setup using the Vector universal testing machine**.**

2.5.1.2 3-point bending test

Using a support span to depth ratio of 16:1, three-point bending tests were performed in compliance with ASTM D7264 to assess the flexural behavior of the composites. A Shimadzu Autograph AGS-X universal testing machine with a maximum load capacity of 10 kN was used to conduct the tests. For every specimen, the flexural strength and related damage modes were investigated. Figure 2.14 shows the test configuration.

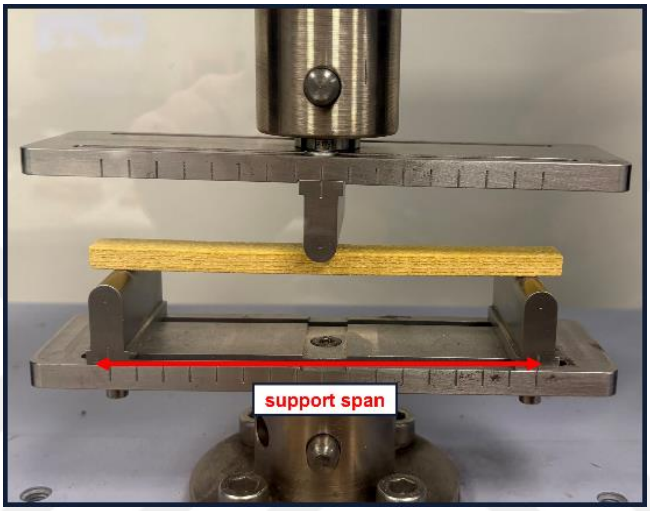

Figure 2.14 : Three-point bending test setup on the Shimadzu universal testing machine**.**

2.5.1.3 Short-beam test

The short-beam shear test was used to assess the interlaminar shear strength for both reference laminate and NP composites. To quickly evaluate delamination behavior, this test was chosen. This technique is similar to the three-point bending test, as shown in Figure 2.15, but it uses thicker specimens and a much shorter support span to encourage interlaminar shear failure. The tests were carried out utilizing a 4:1 support span to depth ratio in compliance with ASTM D2344. A Shimadzu Autograph AGS-X universal testing machine with a maximum load capacity of 10 kN was used to conduct the tests.

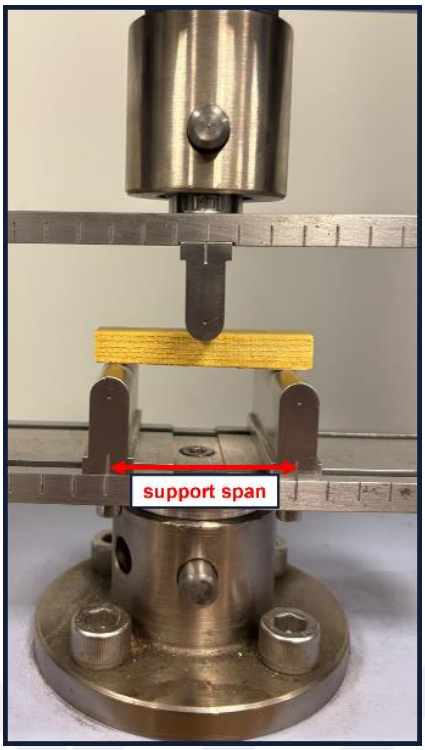

Figure 2.15 : Short-beam shear test setup on the Shimadzu universal testing machine**.**

2.5.2 Torch test for ablation behaviour

Silica–phenolic composite samples were manufactured as 40 mm-diameter circular disks for the ablation test setup shown in Figure 2.16.

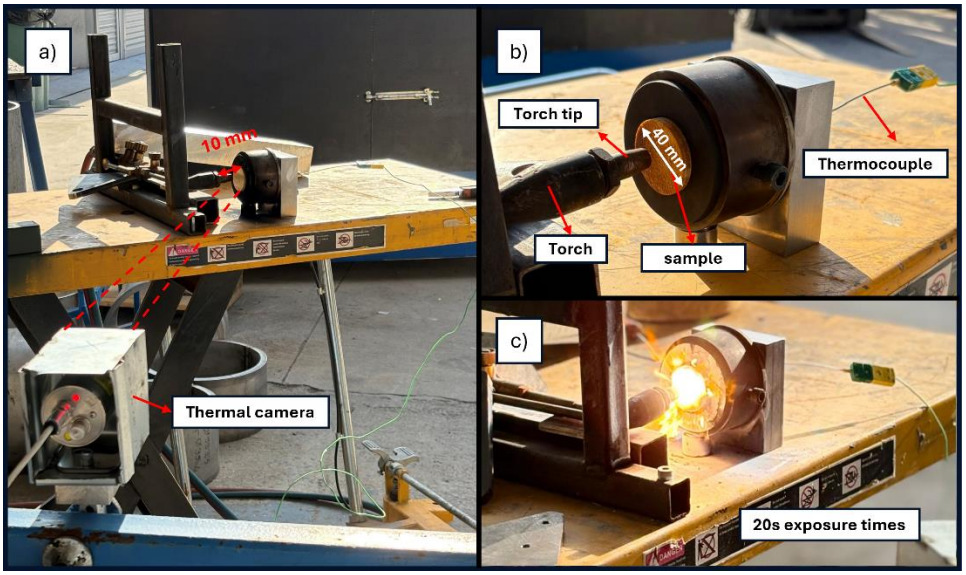

Figure 2.16 : Torch-based ablation test setup with a) thermal camera and b) backside thermocouple instrumentation, and c) representative view of the specimen during torch exposure.

Representative specimens from the reference laminate and the needle-punched configurations (NP-1/1, NP-2/1, and NP-3/1) are shown in Figure 2.17 . Prior to testing, the initial mass and thickness of each specimen were carefully measured. The initial thickness of the specimens ranged from 7.5 to 9.0 mm.

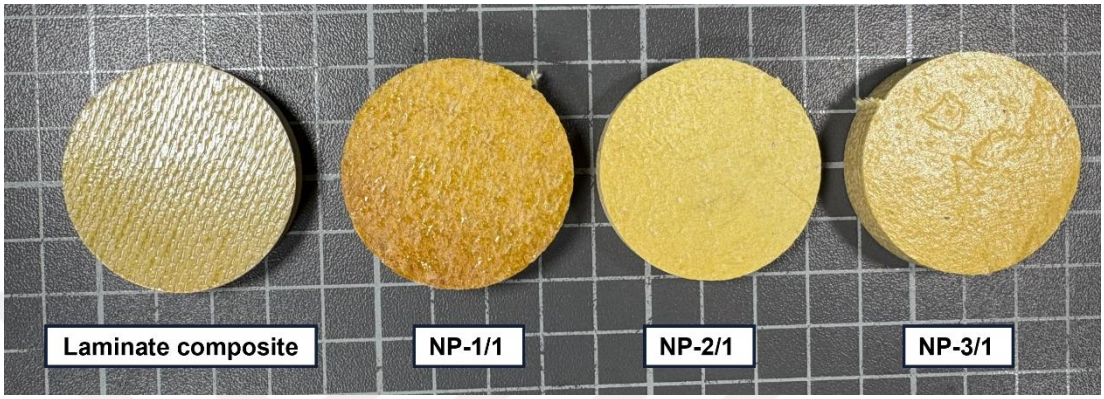

Figure 2.17 : Photograph of 40 mm-diameter silica–phenolic ablation specimens: reference laminated composite and needle-punched configurations (NP-1/1, NP-2/1, NP-3/1).

Samples were positioned in a specially made fixture with a 10 mm space between the sample surface and the torch tip. The heat load was an oxy-propane flame, and each sample was exposed for 20 seconds. During flame exposure, the front surface temperatures were recorded using a thermal camera facing the sample, and the rear surface temperatures were recorded using a thermocouple placed behind the sample. Following the test, the samples' mass and thickness were measured once more. The discrepancies between the original and final values were used to compute the mass ablation rate (based on mass loss) and the linear ablation rate (based on thickness loss). LAR and MAR in Eq. 2.1 and 2.2 can be found using the following formulas.

$$LLinear\ ablation\ rate\ (LAR)(\frac{mm}{s}) = \frac{l_i - l_f}{t_{burn}} \tag{2.1}$$

$$Mass\ ablation\ rate\ (MAR)(\frac{g}{s}) = \frac{m_i - m_f}{t_{burn}} \tag{2.2}$$

where l_i, l_f, m_i and m_f are the thickness and mass of the ablator specimen before and after torch testing, respectively, t_{burn} is ablation time.

3. RESULTS AND DISCUSSION

3.1 Tensile Test Results

Initially, tensile tests were conducted to characterize the in-plane tensile response of the investigated composite configurations. Five specimens were tested for each configuration. As shown in Figure 3.1, the reference laminated composite exhibited the highest tensile strength, reaching approximately 110 MPa.

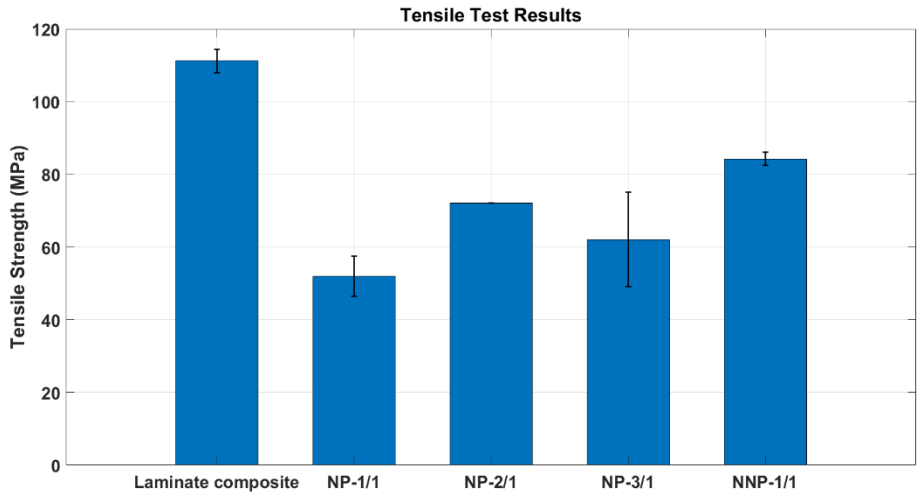

Figure 3.1 : Tensile strength of the laminate, needle-punched (NP-1/1, NP-2/1, NP-3/1) and non-needle-punched (NNP-1/1) HSF/phenolic composites.

A significant decrease in tensile strength was observed in configurations containing felt, especially those with needle punching applied. Samples NP-1/1, NP-2/1, and NP-3/1 showed tensile strengths of approximately 52, 72, and 62 MPa, respectively; these values are approximately 53%, 35%, and 44% lower than the reference laminate. The fabric/felt hybrid structure without needle punching (NNP-1/1) yielded a value of approximately 84 MPa, only 24% lower than the reference laminate. When the NP series is evaluated internally, it is observed that tensile strength tends to increase as the fabric ratio increases; however, no NP configuration reaches the reference laminate level. These results indicate that the needle punching process can negatively affect in-plane load-carrying capacity by creating local fiber breakage/damage and resin-rich

regions in the woven yarns during needle penetration. In addition, discontinuous and thick regions of the felt layer can contribute to the decrease in tensile strength by creating weak zone/stress concentrations at the interfaces. The higher scattering in NP-3/1 points to a behavior more sensitive to production-related variations (local needling density, felt distribution, etc.).

The laminate composite (a) breaks due to a delamination-induced process with noticeable fiber fracture across the thickness, as shown in Figure 3.2.

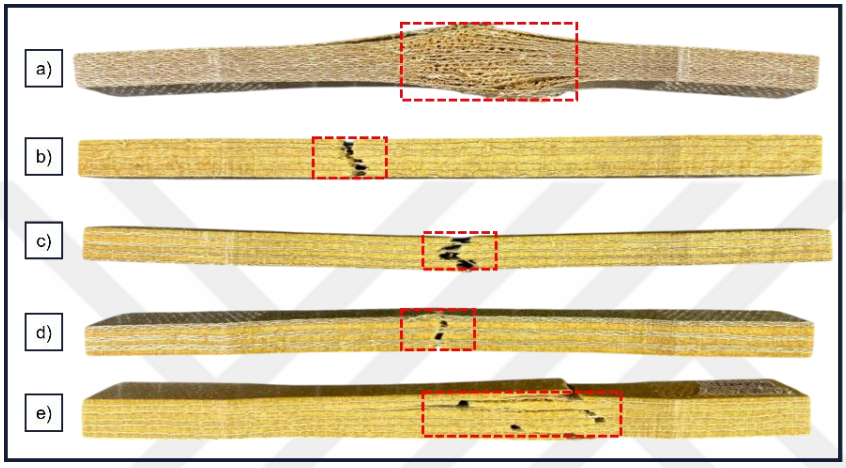

Figure 3.2 : Typical tensile failure modes of HSF/phenolic composites: (a) laminate composite, (b) NP-1/1, (c) NP-2/1, (d) NP-3/1 and (e) NNP-1/1.

NP-1/1 (b) fails by initial fracture of the resin-rich felt region, followed by fibre rupture and pronounced pull-out in the adjacent fabric layers. NP-2/1 (c) exhibits the same trend, with failure starting in the resin-rich felt core and then progressing to fibre rupture/pull-out in the woven plies. In NP-3/1 (d), the continuous three-ply fabric stack leads to a fibre-dominated failure, characterized by rupture of the woven layers in the gauge section and no apparent large-scale delamination. In contrast, the non-needle-punched felt configuration NNP-1/1 (e) exhibits a relatively larger delaminated region concentrated near the mid-span. This damage morphology indicates weaker interfacial bonding between the felt interlayer and the adjacent woven plies. Consistent with the improved interlaminar shear response, the tensile failure images indicate that needle punching shifts the fracture mode from a single dominant delamination band to a more dispersed and fragmented damage pattern by disrupting the continuous layered structure. Tensile tests revealed that needle punching reduces tensile strength by causing localized damage to the woven fabric; however, it visibly reduces layer separation by creating mechanical interlocking and fiber bridging between layers.

3.2 3-Point Bending Test Results

The flexural strengths of the laminate and needle-punched composites are summarized in Figure 3.3. Five specimens were tested for each configuration.

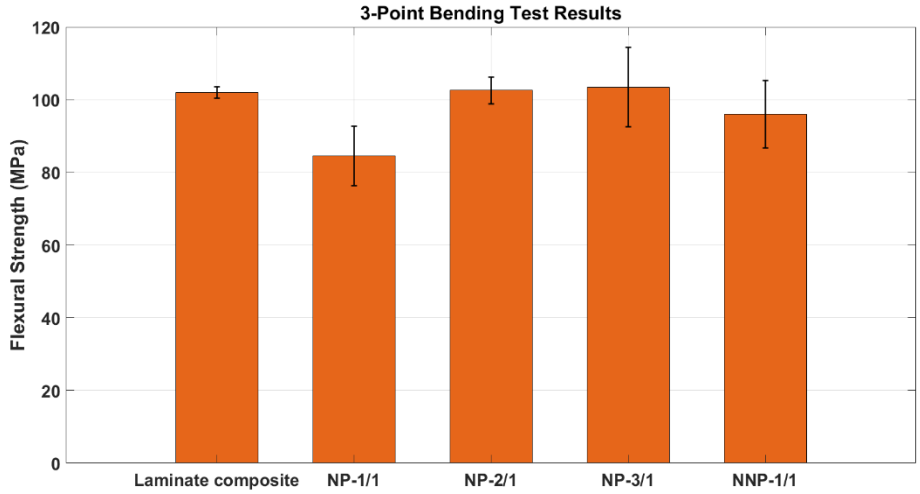

Figure 3.3 : Three-point bending (flexural) strength of laminate, needle-punched (NP-1/1, NP-2/1, NP-3/1) and non-needle-punched (NNP-1/1) HSF/phenolic composites.

The laminate composite exhibits a flexural strength of about 102 MPa. The most aggressive needling configuration (NP-1/1) lowers this value to about 85 MPa (about 17% reduction), whereas NP-2/1 and NP-3/1 largely preserve bending performance, remaining in the about 101–104 MPa range. The non-needle-punched fabric–felt configuration (NNP-1/1) reaches about 96 MPa (about 6% below the laminate) and clearly outperforms NP-1/1. Overall, these results suggest that flexural strength is only moderately influenced by through-thickness needling when sufficient in-plane fabric continuity is retained (NP-2/1 and NP-3/1), indicating that appropriately designed NP architectures can maintain bending load capacity while providing improved through-thickness reinforcement for delamination control. The scatter is relatively low for the laminate, NP-2/1, and NNP-1/1, while NP-1/1 and particularly NP-3/1 show higher variability. In all cases, flexural failure initiates as tensile-side cracking near the mid-span region in the Figure 3.4.

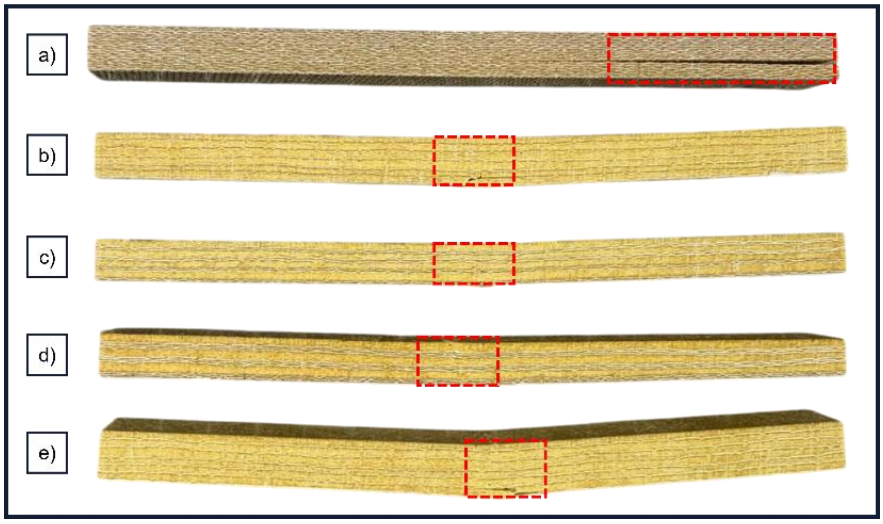

Figure 3.4 : Typical three-point bending failure modes of HSF/phenolic composites: (a) laminate composite, (b) NP-1/1, (c) NP-2/1, (d) NP-3/1 and (e) NNP-1/1.

In the baseline laminate (a), damage concentrates into a wide delaminated region with clear ply separation. NP-1/1 (b) still exhibits interlaminar cracking, but it is confined to a smaller zone. In NP-2/1 and NP-3/1 (c, d), no obvious macroscopic delamination or cracking is observed; the response is dominated by smooth flexural deformation, suggesting mainly diffuse internal matrix microcracking. The non-needle-punched NNP-1/1 specimen (e) shows very limited visible damage, with predominantly global bending deformation and only minor localized indications near mid-span.

3.3 Short-Beam Test Results

Interlaminar shear response was characterized using short-beam tests in the Figure 3.5. While the ILSS in the reference laminated composite was approximately 8 MPa, ILSS values generally increased in configurations containing felt and/or where needle punching was applied. The most significant improvement was obtained in the NP-1/1 sample, with ILSS reaching approximately 11 MPa. In NP-2/1 and NP-3/1 samples, where the fabric ratio increased, ILSS was measured as approximately 9.5 MPa and 8.5 MPa, respectively. The hybrid structure NNP-1/1, which did not undergo needle punching, yielded the highest ILSS value, approximately 11.5–12 MPa. These results demonstrate that the tendency for delamination is reduced and interlayer load transfer is strengthened thanks to the interfacial interaction provided by the felt layer and the Z-directional fiber bridges/mechanical interlocking created by needle punching. The error bars in Figure 3.5 show that scattering is generally limited; however, relatively

higher variability is observed in the reference laminate and NP-3/1 group due to manufacturing-related effects (local consolidation and felt/needle placement).

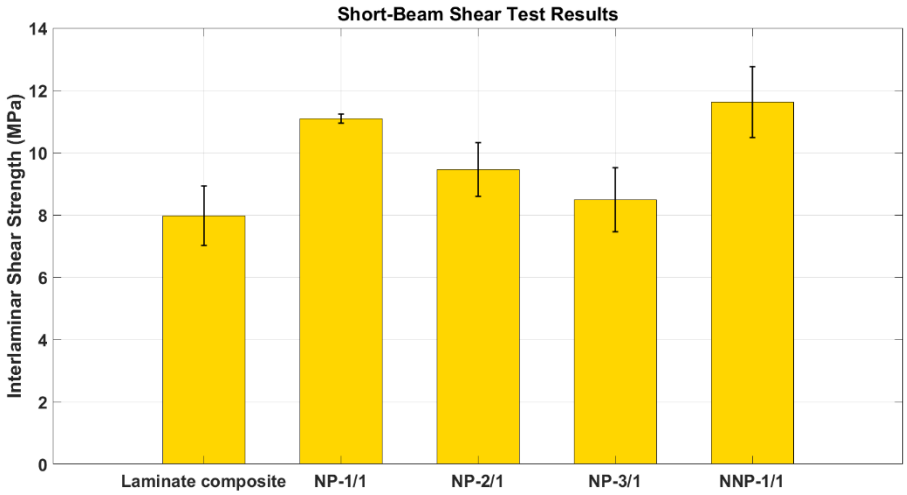

Figure 3.5 : Short-beam interlaminar shear strength of laminate, needle-punched (NP-1/1, NP-2/1, NP-3/1) and non-needle-punched (NNP-1/1) HSF/phenolic composites.

Figure 3.6 compares the damage morphology of the samples after short-beam testing. In the laminate composite (a), the damage is concentrated near the loaded end, where several plies have separated and shifted, forming a distinct shear-dominated damage zone.

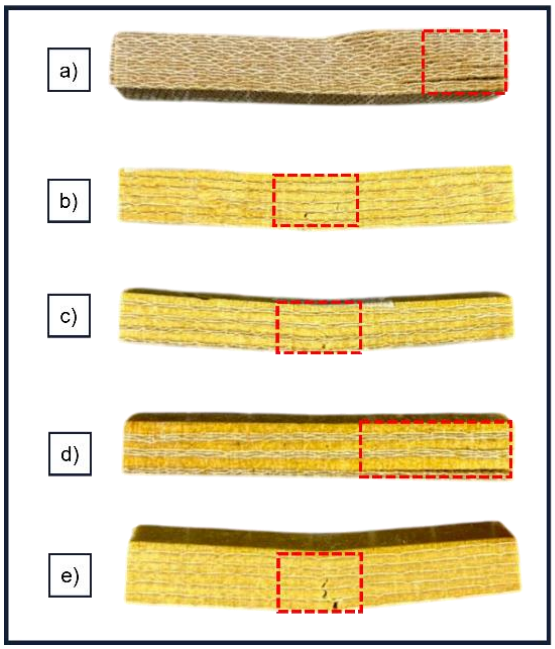

Figure 3.6 : Typical short-beam shear failure modes of HSF/phenolic composites: (a) laminate composite, (b) NP-1/1, (c) NP-2/1, (d) NP-3/1, and (e) NNP-1/1.

In sample NP-1/1 (b), the damage was limited to local cracking in a restricted area in the central region, and no significant delamination was observed. In sample NP-2/1 (c), only slight intralayer/across-layer crack traces are observed in the middle region, and no significant ply separation occurs. In contrast, sample NP-3/1 (d) shows more extensive interlaminar splitting and accompanying limited interlayer slip marks. In sample NNP-1/1 (e), the damage was minimal; apart from a few small cracks in the central region, the laminate integrity was largely preserved. Five specimens were tested for each configuration.

3.4 Torch Test Results

In this section, torch-based ablation performance is assessed in terms of linear ablation rate, mass ablation rate, and post-test damage morphology. Figure 3.7 presents a comparison of the linear and mass ablation rates for the reference laminate , the various needle-punched configurations and non-needle-punched configuration.

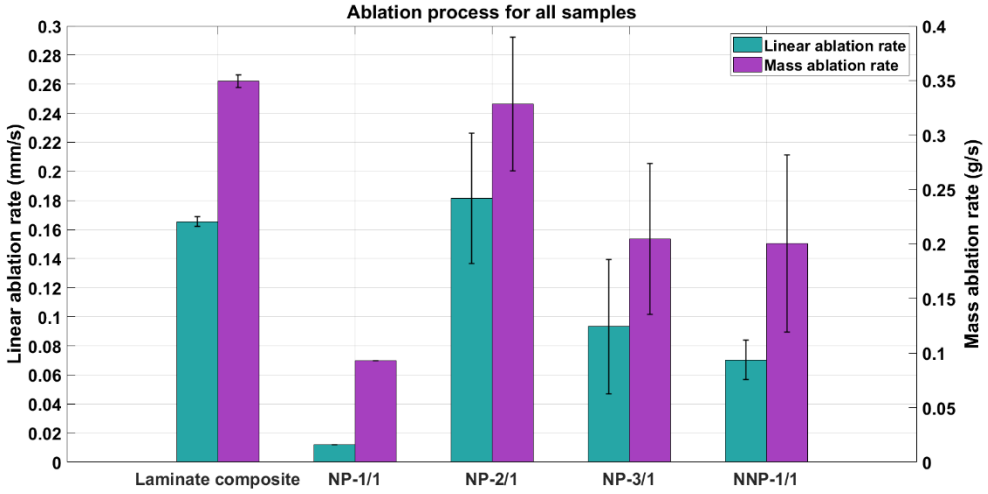

Figure 3.7 : Linear and mass ablation rates of laminate, needle-punched (NP-1/1, NP-2/1, NP-3/1) and non-needle-punched (NNP-1/1) HSF/phenolic composites under 20 s torch exposure.

The reference laminate shows a linear ablation rate of approximately 0.17 mm/s. The NP-1/1 configuration reduces this value to about 0.01 mm/s, corresponding to an approximately 90–95% decrease in linear recession together with roughly 70% lower mass ablation. NP-3/1 also improves ablative performance, lowering the linear rate by approximately 40–50% relative to the laminate, whereas NP-2/1 performs slightly worse than the reference (about 10% higher linear ablation). Overall, the results

suggest that needle punching is most effective in the 1/1 architecture, where alternating fabric and felt layers enable efficient needle penetration and through-thickness interlocking. As the number of consecutive fabric plies between felt layers increases (2/1 and 3/1), the effective z-direction reinforcement appears to weaken. The unexpectedly higher recession of NP-2/1 despite the expectation of improved performance may indicate limited transfer of the needling effect through the thicker fabric block and/or the influence of manufacturing-related non-uniformities (e.g., local variations in needling intensity or resin impregnation). The non-needle-punched fabric–felt configuration (NNP-1/1) also exhibits improved ablation performance, with the linear and mass ablation rates reduced by approximately 60% and 30%, respectively, relative to the laminate. Overall, these findings confirm that a properly designed fabric–felt architecture particularly when combined with effective needle punching can significantly enhance the ablative resistance of HSF/phenolic composites.

Figure 3.8 presents the post-test specimens in (a) front view and (b) side view. The red dashed circles highlight the ablation center, indicating the region of maximum surface recession and damage. In keeping with its high linear and mass ablation rates, the laminate composite displays a broad ablation center with severe ply peeling and extensive delamination, as seen in Figure 3.8.

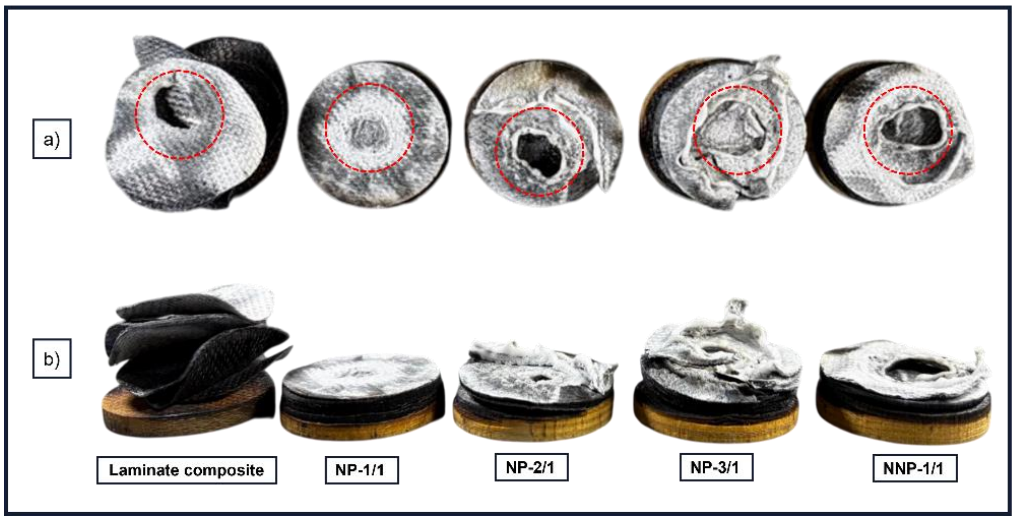

Figure 3.8 : Post-ablation morphologies of HSF/phenolic composites: (a) front views and (b) side views of laminate, NP-1/1, NP-2/1, NP-3/1 and NNP-1/1 specimens.

In the side view (Figure 3.8b), the charred layer and the underlying virgin material are clearly distinguishable, which is consistent with the strong thermal gradient observed during testing. While surface temperatures reached around 2400 °C, the back-face thermocouple recorded only about 73 °C, approximately 50 °C above ambient.. The outer char layer appears as a porous, fragile region formed after resin decomposition, whereas the virgin layer retains its original dense structure, indicating the unreacted core. The thickness and continuity of the char layer also provide a direct indication of the extent of thermal degradation. Compared to the reference laminate, the NP-1/1 sample formed a more compact and highly integrated char layer, the ablation core remained smaller, and no significant layer separation was observed in the lateral view. In the NP-2/1 specimen, the ablation pit was deeper and more irregular, with scattered char spallation; this morphology is consistent with poor ablation performance. A thicker and more porous char layer formed in the NP-3/1 sample, and traces of layer separation were observed in the area near the ablation site; this indicates that the needling effect may negatively impact structural integrity under certain conditions. The NNP-1/1 structure, which was not subjected to needle punching, exhibited an intermediate morphology with a moderate depression and limited layer separation. In general, it appears that ablation behavior under torch loading is affected not only by thermochemical resistance but also by the structural integrity of the char layer; weak interlayer bonding leads to the rupture/shedding of larger char particles, increasing mass loss.

4. CONCLUSION

In this study, the mechanical and ablative performance of HSF/phenolic composites manufactured in laminated, needle-punched (NP), and non-needle-punched fabric–felt (NNP) configurations was systematically evaluated. Tensile testing indicated that through-thickness reinforcement introduced by needle punching generally reduces tensile strength, with the magnitude of the reduction depending on the stacking sequence; in contrast, the non-needle-punched fabric–felt configuration (NNP-1/1) retained a substantial portion of the laminate tensile capacity. Flexural response was comparatively less sensitive to configuration: NP-2/1 and NP-3/1 largely preserved, and in some cases slightly exceeded, the reference laminate flexural strength, whereas NP-1/1 showed a moderate decrease and NNP-1/1 remained close to the baseline. Short-beam shear results highlighted the key benefit of through-thickness configurations, showing increased interlaminar shear strength in all reinforced configurations most notably for NP-1/1 and NNP-1/1 thereby indicating improved delamination resistance relative to the laminate.

Torch tests under severe oxy–propane exposure further demonstrated that architecture strongly governs ablation behavior. While surface temperatures approached approximately 2400 °C, the back-face thermocouple measured only about 73 °C, corresponding to an increase of roughly 50 °C above ambient. Among the investigated designs, NP-1/1 exhibited the most favorable performance, with the largest reduction in both linear abaltion rate and mass abaltion rate. NP-3/1 and NNP-1/1 provided intermediate improvements, whereas NP-2/1 unexpectedly showed higher recession than the reference laminate. This deviation is likely due to manufacturing variability, and increasing the number of specimens is expected to yield a more representative result for NP-2/1.

Overall, the results indicate that ablation performance is governed by the combined effect of thermochemical resistance and the physical integrity of the material/char structure. Among the investigated designs, the NP-1/1 architecture provides the most effective use of needle punching in HSF/phenolic systems, delivering improved interlaminar shear resistance and superior ablation protection, albeit with a reduction

in in-plane tensile strength. The NNP-1/1 configuration also appears to be a viable alternative, offering simpler manufacturing while maintaining competitive mechanical and ablative performance. Future work will focus on optimizing needling parameters and processing conditions, as well as needle geometry and felt characteristics, and on developing hybrid preform concepts that integrate laminated and needled regions to better tailor the trade-off between in-plane load capacity, delamination resistance, and ablative efficiency for aerospace TPS applications.

REFERENCES

[1] **AJ, A. J., Panigrahi, S. K., Sasikumar, P., Rao, K. S., & Krishnakumar, G.** (2022). Ablative properties, thermal stability, and compressive behaviour of hybrid silica phenolic ablative composites. *Polymer Degradation and Stability*, *203*, 110063.

[2] **Shi, S., Liang, J., & He, R.** (2015). Thermal decomposition behavior of silica-phenolic composite exposed to one-sided radiant heating. *Polymer composites*, *36*(8), 1557-1564.

[3] **Adams, M. C.** (1959). Recent advances in ablation. *ARS Journal*, *29*(9), 625-632.

[4] **Natali, M., Kenny, J. M., & Torre, L**. (2016). Science and technology of polymeric ablative materials for thermal protection systems and propulsion devices: A review. *Progress in Materials Science*, *84*, 192-275.

[5] **Sutton, G. P., & Biblarz, O.** (2011). *Rocket propulsion elements*. John Wiley & Sons.

[6] **Schmidt, D. L.** (1969). Ablative polymers in aerospace technology. *Journal of Macromolecular Science—Chemistry*, *3*(3), 327-365.

[7] **Kumar, C.V. and Kandasubramanian, B.** (2019). Ind. Eng. Chem. Res. 58 (51): 22663–22701.

[8] **Sayir, A.** (2004). Carbon fiber reinforced hafnium carbide composite. *Journal of materials science*, *39*(19), 5995-6003.

[9] **Yehia, A. A., Akelah, A. M., Rehab, A., El-Sabbagh, S. H., El Nashar, D. E., & Koriem, A. A.** (2012). Evaluation of clay hybrid nanocomposites of different chain length as reinforcing agent for natural and synthetic rubbers. *Materials & Design*, *33*, 11-19.

[10] **El-Nemr, K. F.** (2011). Effect of different curing systems on the mechanical and physico-chemical properties of acrylonitrile butadiene rubber vulcanizates. *Materials & Design*, *32*(6), 3361-3369.

[11] **Donskoy, A.A.** (1995). In: New Approaches to Polymer Materials, 1e (ed. G.E. Zaikov), 53–92. Hauppauge, NY: Nova Publishers.

[12] **Kumar, C. V., & Kandasubramanian, B.** (2019). Advances in ablative composites of carbon-based materials: a review. *Industrial & Engineering Chemistry Research*, *58*(51), 22663-22701.

[13] **Li, Y., Mao, C., Wu, F., Xue, C., & Zhang, C.** (2025). Thermal insulation performance of high-silica/phenolic composites: Experimental and numerical study. *Composite Structures*, 119855.

[14] **Uyanna, O., & Najafi, H.** (2020). Thermal protection systems for space vehicles: A review on technology development, current challenges and future prospects. Acta Astronautica, 176, 341-356.

[15] **Friedman, H. L.** (1964). Kinetics of thermal degradation of char-forming plastics from thermogravimetry. Application to a phenolic plastic. I*n Journal of polymer science part C: polymer symposia* (Vol. 6, No. 1, pp. 183-195). New York: Wiley Subscription Services, Inc., A Wiley Company.

[16] **Kratsch, K., Hearne, L., & McChesney, H.** (1963). Thermal performance of heat shield composites during planetary entry. *In Engineering Problems of Manned Interplanetary Exploration* (p. 1515).

[17] **Beecher, N., & Rosensweig, R. E.** (1961). Ablation mechanisms in plastics with inorganic reinforcement. *ARS journal*, *31*(4), 532-539.

[18] **Dimitrienko, Y. I.** (2016). *Thermomechanics of composite structures under high temperatures* (Vol. 224). Berlin: Springer.

[19] **Trick, K. A., & Saliba, T. E.** (1995). Mechanisms of the pyrolysis of phenolic resin in a carbon/phenolic composite. *Carbon*, *33*(11), 1509-1515.

[20] **Wallenberger, F. T.** (1999). Structural silicate and silica glass fibers. In *Advanced inorganic fibers: process-structure-properties-applications* (pp. 129-168). Boston, MA: Springer US.

[21] **Duffa, G.** (2013). *Ablative thermal protection systems modeling*. American Institute of Aeronautics and Astronautics, Inc..

[22] **Koo, J., Ho, W., Bruns, M., & Ezekoye, O.** (2006, July). A Review of Numerical and Experimental Characterization of Thermal Protection Materials: Part III-Material Testing. In *43rd AIAA/ASME/SAE/ASEE Joint Propulsion Conference & Exhibit* (p. 5773).

[23] **Knop, A., & Pilato, L. A.** (2013). *Phenolic resins: chemistry, applications and performance*. Springer Science & Business Media.

[24] **Asaro, L., Manfredi, L. B., & Rodriguez, E. S.** (2018). Study of the ablative properties of phenolic/carbon composites modified with mesoporous silica particles. *Journal of Composite Materials*, *52*(30), 4139-4150.

[25] **Ding, J., Huang, Z., Qin, Y., Shi, M., Huang, C., & Mao, J.** (2015). Improved ablation resistance of carbon–phenolic composites by introducing zirconium silicide particles. *Composites Part B: Engineering*, *82*, 100-107.

[26] **Huang, Y., Liu, Z., Yan, L., Zou, H., Chen, Y., & Liang, M.** (2023). Enhanced ablation resistance of phenolic composites through the construction of a sea-island nanostructured char layer via in-situ catalytic graphitization of incorporated Salen-Ni complex. *Chemical Engineering Journal*, *464*, 142651.

[27] **Park, J. M., Kwon, D. J., Wang, Z. J., Roh, J. U., Lee, W. I., Park, J. K., & DeVries, K. L.** (2014). Effects of carbon nanotubes and carbon fiber reinforcements on thermal conductivity and ablation properties of carbon/phenolic composites. *Composites Part B: Engineering*, *67*, 22-29.

[28] **Chen, Y., Chen, P., Hong, C., Zhang, B., & Hui, D.** (2013). Improved ablation resistance of carbon–phenolic composites by introducing zirconium diboride particles. *Composites Part B: Engineering*, *47*, 320-325.

[29] **Wang, S., Huang, H., Tian, Y., & Huang, J.** (2020). Effects of SiC content on mechanical, thermal and ablative properties of carbon/phenolic composites. *Ceramics International*, *46*(10), 16151-16156.

[30] **Schultz, F. E.** (1966). *Investigation of the Effect of Material Properties on Composite Ablative Material Behavior* (Third Quarterly Report). NASA CR-71295.

[31] **Elwan, I., Jabra, R., & Arafeh, M. H.** (2018). Preparation and ablation performance of lightweight phenolic composite material under oxyacetylene torch environment. *Journal of Aerospace Technology and Management*, *10*, e3118.

[32] **AJ, A. J., Panigrahi, S. K., Sasikumar, P., Rao, K. S., & Krishnakumar, G.** (2022). Ablative properties, thermal stability, and compressive behaviour of hybrid silica phenolic ablative composites. *Polymer Degradation and Stability*, *203*, 110063.

[33] **Koo, J. H., & Pilato, L. A.** (2020). Polymer Nanocomposite Ablatives− Part Ii. *International Journal of Energetic Materials and Chemical Propulsion*, *19*(2).

[34] **Wang, X., Xu, Q., Zheng, Q., Shao, Y., & Shen, J.** (2025). Reviews of Fiber-Reinforced Phenolic Resin-Based Thermal Protection Materials for Aircraft. *Energies (19961073)*, *18*(4).

[35] **Feldman, J. D., Venkatapathy, E., Wilkinson, C., & Mercer, K. J.** (2015). *Development of an ablative 3D quartz/cyanate ester composite for the orion spacecraft compression pad* (No. ARC-E-DAA-TN26391).

[36] **Jiang, Z., Wang, T., Li, W., & Zhang, Z.** (2023). Effect of weaving parameter and resin structure of lightweight integrated multifunctional composite on thermal protection performance in extreme environment. *PolymerComposites*, *44*(8),45094518.

[37] **Blaiszik, B. J., Kramer, S. L., Olugebefola, S. C., Moore, J. S., Sottos, N. R., & White, S. R.** (2010). Self-healing polymers and composites. *Annual review of materials research*, *40*(1), 179-211.

[38] **Mudra, E.; Koribanich, I.; Hrubovˇcáková, M.; Shepa, I.; Kovalcikova, A.; Dusza, J.** Preparation and Fracture Analysis of Advanced Layered Composite with Graphene-Coated Alumina Nanofibers. J. Nano Res. 2023, 78, 17–22.

[39] **Panasiuk, K., & Dudzik, K.** (2022). Determining the stages of deformation and destruction of composite materials in a static tensile test by acoustic emission. *Materials*, *15*(1), 313.

[40] **Huang, T., & Bobyr, M.** (2023). A review of delamination damage of composite materials. *Journal of Composites Science*, 7(11), 468.

[41] **Hutchinson, J. W., & Lu, T. J.** (1995). Laminate delamination due to thermal gradients. *Journal of engineering materials and technology*, 117(4), 386-390.

[42] **Yin, W.-L.** (1997). The effect of temperature gradient on the free-edge interlaminar stresses in multi-layered structures. *Journal of Composite Materials*, 31(24), 2460–2477.

[43] **Sørensen, B. F.** (2002). Thermally induced delamination of symmetrically graded multilayers. *Journal of the American Ceramic Society*, *85*(4), 858–864.

[44] **Huang, T., & Bobyr, M.** (2023). A review of delamination damage of composite materials. *Journal of Composites Science*, *7*(11), 468.

[45] **Stackpoole, M., Gasch, M., Venkatapathy, R., & Ellerby, D.** (2022, March). *The state of the art: Ablative thermal protection systems* [Conference presentation]. Additive Manufacturing TPS Workshop, Houston, TX, United States. NASA Ames Research Center.

[46] **Carlsson, L. A., Adams, D. F., & Pipes, R. B.** (2013). Basic experimental characterization of polymer matrix composite materials. *Polymer Reviews*, *53*(2), 277-302.

[47] **Hasan, K. F., Horváth, P. G., & Alpár, T.** (2021). Potential fabric-reinforced composites: a comprehensive review. *Journal of Materials Science*, 56(26), 14381-14415.

[48] **Chowdhury, I. R., & Summerscales, J.** (2024). Woven fabrics for composite reinforcement: A review. *Journal of Composites Science*, 8(7), 280.

[49] **Elmogahzy, Y.** (2019). *Engineering textiles: Integrating the design and manufacture of textile products*. Woodhead Publishing.

[50] **Adanur, S.** (2020). *Handbook of weaving*. CRC press.

[51] **Cox, B. N., & Flanagan, G.** (1997). Handbook of analytical methods for textile composites (No. NASA-CR-4750).

[52] **Akyazici, Z. N., Sahin, I. H., Dincer, M., Sudutemiz, Y. C., & Cebeci, H.** (2024). Establishing Architectural Effects of Variable Binder on 3D Orthogonal Woven Composites: RVE Model and Experiment Validation. In *AIAA SCITECH 2024 Forum* (p. 2285).

[53] **Dang, D. Z., Stern, E. C., & Boyd, I. D.** (2021). Inferring thermal conductivity of a dual-layer woven thermal protection system using cross-validation. *Thermal Science and Engineering Progress*, *23*, 100904.

[54] **Ellerby, D. T., Venkatapathy, E., Gasch, M. J., Kazemba, C., Mahzari, M., Milos, F. S., & Stackpoole, M**. (2019, September). *Heatshield for Extreme Entry Environment Technology (HEEET) thermal protection system (TPS).* MS&T19 – Materials Science & Technology Conference and Exhibition, Portland, OR, United States.

[55] **Liang, H., Li, W., Wang, T., Wang, L., Yang, G., & Guo, J.** (2023). Optimal design of three-dimensional thermal protection structure considering orthotropic properties of woven composites based on Micro-CT image. *International Journal of Thermal Sciences*, 191, 108579.

[56] **Bednarcyk, B. A., Ricks, T. M., Pineda, E. J., Murthy, P. L., Mital, S. K., Hu, Z., & Gustafson, P. A.** (2022). Thermal conductivity of 3D woven composite thermal protection system materials via multiscale recursive micromechanics. In *AIAA SCITECH 2022 Forum* (p. 2280).

[57] **Chen, X., Chen, L., Zhang, C., Song, L., & Zhang, D.** (2016). Three-dimensional needle-punching for composites–A review. *Composites Part A: Applied science and manufacturing*, *85*, 12-30.

[58] **Xie, J., Liang, J., Fang, G., & Chen, Z.** (2015). Effect of needling parameters on the effective properties of 3D needled C/C-SiC composites. *Composites Science and Technology*, *117*, 69-77.

[59] **Kang, T. J., Jung, K. H., Park, J. K., Youn, J. R., & Lee, S. G.** (2002). Effect of punching density on the mechanical and thermal properties of needle-punched nonwoven carbon/phenolic composites. *Polymers and Polymer Composites*, *10*(7), 521-530.

[60] **Ajmeri, J. R., & Ajmeri, C. J.** (2016). Developments in nonwoven as geotextiles. In *Advances in technical nonwovens* (pp. 339-363). Woodhead Publishing.

[61] **Qi, Y., Fang, G., Wang, Z., Liang, J., & Meng, S.** (2020). An improved analytical method for calculating stiffness of 3D needled composites with different needle-punched processes. *Composite Structures*, *237*, 111938.

[62] **Wang, K., Xu, C., Gao, B., Zhao, X., Wang, B., & Meng, S.** (2025). Damage evolution and failure behavior of 3D needled Carbon/Carbon composites under compressive at ultra-high temperatures up to 2800° C. *Journal of the European Ceramic Society*, *45*(6), 117183

[63] **Chen, Y., Tao, R., & Mao, Y.** (2024). Thermal reaction based mesoscale ablation model for phase degradation and pyrolysis of needle-punched composite. *Composites Science and Technology*, *258*, 110898.

[64] **Qian, Z., Cai, H., Cao, J., Wang, P., Li, L., Cao, Y., ... & Long, D.** (2022). 3D needle-punched carbon/quartz fabric reinforced nanoporous phenolic composites with co-optimized mechanics, insulation and ablation. *Composites Communications*, *36*, 101393.

[65] **Cai, H., Niu, B., Qian, Z., Li, T., Wang, P., Li, L., ... & Long, D.** (2024). Mechanical, thermal insulation, and ablation behaviors of needle-punched fabric reinforced nanoporous phenolic composites: the role of anisotropic microstructure. *Composites Science and Technology*, *245*, 110325.

[66] **Cai, H., Qian, Z., Li, L., Zhang, Y., Niu, B., & Long, D.** (2023). Tensile behaviors of nanoporous phenolic composites reinforced by 3D needle-punched preforms with different weave patterns. *Composites Communications*, *43*, 101700.

[67] **Jabbar, A., Ahmad, A., Adnan, M., Nawab, Y., Javed, Z., & Irfan, M.** (2021). Enhanced interlaminar shear and impact performance of woven carbon/epoxy composites interleaved with needle punched high performance polyethylene fiber nonwoven. *Journal of Applied Polymer Science*, *138*(25), 50683.

[68] **Shi, S., Gong, C., Liang, J., Fang, G., Wen, L., & Gu, L.** (2016). Ablation mechanism and properties of silica fiber-reinforced composite upon oxyacetylene torch exposure. *Journal of Composite Materials*, *50*(27), 3853-3862.

[69] **McDermott, R.** (2018). *Exploration of a New Affordable Thermal Protection System Utilizing Needle-Punched (2.5 D) Fabric Composites* (Doctoral dissertation).

[70] **Balasubramanian, K., Sultan, M. T., & Rajeswari, N.** (2018). Manufacturing techniques of composites for aerospace applications. In *Sustainable composites for aerospace applications* (pp. 55-67). Woodhead Publishing.

[71] **Hou, T. H., Bai, J. M., & Baughman, J. M.** (2006). Processing and properties of a phenolic composite system. *Journal of reinforced plastics and composites*, *25*(5), 495-502.

[72] **Pupin, C., Ross, A., Dubois, C., Rietsch, J. C., & Ruiz, E.** (2017). Predicting porosity formation in phenolic resins for RTM manufacturing: The porosity map. Composites Part A: Applied Science and Manufacturing, 100, 294-304.

[73] **Caporale, A. M., Airoldi, A., Natali, M., Boiocchi, M., Torre, L., & Rallini, M.** (2022). Thermomechanical response of out-of-autoclave infused carbon-phenolic laminates for rocket engine applications subjected to surface ablation. *Composites Part A: Applied Science and Manufacturing*, *159*, 107035.

[74] **Basingala, P. K., & Neigapula, V. S. N.** (2024). Enhancement of mechanical and thermal properties of carbon fiber phenolic resin composites using silicon carbide filler for thermal protection system applications. *Journal of Industrial Textiles*, *54*, 15280837241263312.

[75] **Sha, Z., Yang, W., Wang, C., Islam, M. S., Yeoh, G. H., Officer, D. L., ... & Wang, C. H. (2024).** Enhancing oxidation resistance of carbon fibre reinforced phenolic composites by ZrO2 nanoparticles through out-of-autoclave vacuum infusion. *Composites Part A: Applied Science and Manufacturing*, *180*, 108071.

CURRICULUM VITAE

Name Surname **:** Zeynep Nur AKYAZICI

EDUCATION **:**

- **B.Sc.** **:** 2021, Istanbul Technical University, Faculty of Textile Technologies and Design, Textile Engineering Department
- **M.Sc.** **:** 2026, Istanbul Technical University, Faculty of Aeronautical and Astronautical Engineering, Aeronautical and Astronautical Engineering Programme

PROFESSIONAL EXPERIENCE AND REWARDS:

- First in the department, 2021
- ITU Aerospace Research Center (ITU ARC)-Nanomaterials, Textiles and Advanced Composites Research Group
  Student Researcher, August 2022-June 2024
- DeltaV Space Technologies
  R&D Engineer, January 2025-Today

PUBLICATIONS, PRESENTATIONS AND PATENTS ON THE THESIS:

- **Akyazici, Z. N.,** Sahin, I. H., Dincer, M., Sudutemiz, Y. C., & Cebeci, H. (2024). Establishing Architectural Effects of Variable Binder on 3D Orthogonal Woven Composites: RVE Model and Experiment Validation. In *AIAA SCITECH 2024 Forum* (p. 2285).
- **Akyazici, Z. N.,** Selamet, B., Kilinc, M. E., Baysal, M., Eken, S., Tola, C., & Kahraman, M. (2026). Evaluation of Ablation and Mechanical Behavior in Needle-Punched High Silica-Phenolic Composites With Comparison to Laminated Structures. In *AIAA SCITECH 2026 Forum* (p. 1778).

OTHER PUBLICATIONS, PRESENTATIONS AND PATENTS:

- Arslan, D., Dincer, M., **Akyazici, Z. N.,** Kucukkalfa, E., Demirer, E. R., Yildiz, K., ... & Cebeci, H. IN-SITU CURE MONITORING OF 3D WOVEN COMPOSITES WITH A MULTIFUNCTIONAL CNT SENSOR.

- Karabal, M., Dincer, M., Arslan, D., Yüksel, R., **Akyazici, Z. N.,** Yildiz, A., & Cebeci, H. (2024). Direct 3D printing of strain sensors onto 3D woven orthogonal composite structures: Evaluating two distinct approaches for sensor performance. In *AIAA SCITECH 2024 Forum* (p. 2284).